P. mirabilis-derived pore-forming haemolysin, HpmA drives intestinal alpha-synuclein aggregation in a mouse model of neurodegeneration

Eugene Huh,[a,b,l,m] Jin Gyu Choi,[a,l,n] Yujin Choi,[c] In Gyoung Ju,[a,b] Bora Kim,[b] Yoon-Jung Shin,[b] Jong Min An,[d] Myoung Gyu Park,[e] Sung Vin Yim,[f] Su Jin Chung,[g] Sang-Uk Seo,[h] Dokyoung Kim,[d,i] Chun Hyung Kim,[j] Dong Hyun Kim,[b] and Myung Sook Oh[a,b,c,k,*]

[a]Department of Oriental Pharmaceutical Science and Kyung Hee East-West Pharmaceutical Research Institute, College of Pharmacy, Kyung Hee University, 26, Kyungheedae-ro, Dongdaemun-gu, Seoul, 02447, Republic of Korea
[b]Neurobiota Research Center, College of Pharmacy, Kyung Hee University, 26, Kyungheedae-ro, Dongdaemun-gu, Seoul, 02447, Republic of Korea
[c]Department of Biochemical and Pharmaceutical Sciences, Graduate School, Kyung Hee University, 26, Kyungheedae-ro, Dongdaemun-gu, Seoul, 02447, Republic of Korea
[d]Department of Biomedical Science, Graduate School, Kyung Hee University, 26 Kyungheedae-ro, Dongdaemun-gu, Seoul, 02447, Republic of Korea
[e]MetaCen Therapeutics Inc. R&D Center, 256 Changryongdae-ro, Yeongtong-gu, Suwon-si, Gyeonggi-Do, 16229, Republic of Korea
[f]Department of Clinical Pharmacology and Therapeutics, College of Medicine, Kyung Hee University, 26 Kyungheedae-ro, Dongdaemun-gu, Seoul, 02447, Republic of Korea
[g]Department of Neurology, Myongji Hospital, Hanyang University College of Medicine, 155 Hwasu-ro, Deokyang-gu, Goyang-si, Gyeonggi-Do, 10475, Republic of Korea
[h]Department of Microbiology, College of Medicine, The Catholic University of Korea, 222 Banpodae-ro, Seocho-gu, Seoul, 06591, Republic of Korea
[i]Department of Anatomy and Neurobiology, College of Medicine, Kyung Hee University, 26 Kyungheedae-ro, Dongdaemun-gu, Seoul, 02447, Republic of Korea
[j]Paean Biotechnology, 17 Techno 4-ro, Yuseong-gu, Daejeon, 34013, Republic of Korea
[k]Department of Integrated Drug Development and Natural Products, Graduate School, Kyung Hee University, 26 Kyungheedae-ro, Dongdaemun-gu, Seoul, 02447, Republic of Korea

eBioMedicine
2023;98: 104887
Published Online 22 November 2023
https://doi.org/10.1016/j.ebiom.2023.104887

Summary

Background Recent studies suggesting the importance of the gut-microbiome in intestinal aggregated alpha synuclein (α-syn) have led to the exploration of the possible role of the gut-brain axis in central nervous system degeneration. *Proteus mirabilis* (*P. mirabilis*), a gram-negative facultative anaerobic bacterium, has been linked to brain neurodegeneration in animal studies. We hypothesised that *P. mirabilis*-derived virulence factors aggregate intestinal α-synuclein and could prompt the pathogenesis of dopaminergic neurodegeneration in the brain.

Methods We used vagotomised- and antibiotic-treated male murine models to determine the pathogenesis of *P. mirabilis* during brain neurodegeneration. The neurodegenerative factor that is driven by *P. mirabilis* was determined using genetically mutated *P. mirabilis*. The pathological functions and interactions of the virulence factors were determined *in vitro*.

Findings The results showed that *P. mirabilis*-induced motor dysfunction and neurodegeneration are regulated by intestinal α-syn aggregation in vagotomised- or antibiotic-treated murine models. We deduced that the specific virulence factor, haemolysin A (HpmA), plays a role in the pathogenesis of *P. mirabilis*. HpmA is involved in α-synuclein oligomerisation and membrane pore formation, resulting in the activation of mTOR-mediated autophagy signalling in intestinal neuroendocrine cells.

Interpretation Taken together, the results of the present study suggest that HpmA can interact with α-syn and act as a possible indicator of brain neurodegenerative diseases that are induced by *P. mirabilis*.

*Corresponding author. Department of Biochemical and Pharmaceutical Sciences, Graduate School, Kyung Hee University, 26 Kyungheedae-ro, Dongdaemun-gu, Seoul 02447, Republic of Korea.
E-mail address: msohok@khu.ac.kr (M.S. Oh).
[l]These authors have contributed equally to this work.
[m]Current address: Department of Formulae Pharmacology, College of Korean Medicine, Gachon University, 1342 Seongnamdae-ro, Sujung-Gu, Seongnam, Gyeonggi-Do, 13120, Republic of Korea.
[n]Current address: MThera Pharma Co., 1 Magokjungang 8-ro, Gangseo-gu, Seoul, 07793, Republic of Korea.

Funding This study was supported by a grant from the National Research Foundation of Korea.

Keywords: Microbiota-gut-brain axis; Neurodegenerative disease; Alpha-synuclein; *Proteus mirabilis*; Haemolysin A; Pore formation

Research in context

Evidence before this study

The gut-brain axis has been conceptualised to contribute to the pathogenesis of Parkinson's disease (PD) based on the Braak hypothesis as alpha-synuclein (α-syn) propagates from the gut to the brain. *Proteus mirabilis* (*P. mirabilis*, 2 x 10^8 CFU per mouse for 5 days), a gram-negative facultative anaerobic bacterium, causes brain neurodegeneration.

Added value of this study

Haemolysin A (HpmA), derived from *P. mirabilis* oligomerises with α-syn and itself, activates mTOR-mediated autophagy signalling in intestinal cells, and induces brain α-syn accumulation and neurodegeneration in a mouse model of PD.

Implications of all the available evidence

HpmA may be involved in PD development and could, therefore, be an important target for future treatments or a biomarker of PD.

Introduction

Parkinson's disease (PD), a brain neurodegenerative disease, manifests with motor dysfunction accompanied by dopamine deficits and alpha synuclein (α-syn) inclusion in the brain. Since PD diagnosis occurs in the late stage of progression, markers of the prodromal stages, including rapid eye movement sleep behaviour disorders, olfactory loss, autonomic dysfunction and constipation are considered observable and predictive of clinical PD.[1,2]

During the prodromal stage, various non-motor symptoms may appear and are closely related to the peripheral nervous systems (PNS) as well as the brain's central nervous system (CNS). Based on Braak's hypothesis, which suggests that pathological α-syn ascends from the enteric nervous system (ENS)-innervating vagal fibres to the inferior ganglia of the vagus nerve and brainstem nuclei, mounting evidence suggests that the pathology of PD may originate earlier in the gastrointestinal (GI) tract before progressing in the brain.[3,4] There is epidemiological evidence that complete vagotomy may decrease the prevalence of PD.[5,6] In pre-clinical studies, accumulating evidence shows that α-syn fibrils could progress from the vagus nerve that innervates the gut to the midbrain in a retrograde axonal transport or prion-like manner and cause behavioural dysfunction.[7–10] Based on clues that PD may originate in the gut, several studies present a challenging hypothesis that PD comprises distinct subtypes: a gut-first (PNS-based) subtype and a brain-first (CNS-based) subtype.[11,12]

The microbiota-gut-brain axis (MGB axis) plays a role in the maintenance of brain physiological functions as well as in the pathological progression of PD.[13,14] The gut is colonised by numerous microbiomes which affect the development and pathophysiological responses of the nervous system. It has been hypothesised that alterations in the gut microbiota composition may disrupt the intestinal barrier and trigger pathological peripheral enteric neuronal responses, which could contribute to neurodegeneration in the CNS. In addition, several bacterial-derived factors abrogate PD progression. For example, Lipopolysaccharide (LPS) produced by the gut microbiota induced a significant disruption in tight junction proteins in the intestine of α-syn overexpressing mice, indicating that there is an interaction between gut microbiota and PD development.[15] In addition to LPS, the gut microbiota may also affect α-syn aggregation through virulence factors. Amyloid proteins are produced by several microorganism, including *Escherichia coli*, which produces curli amyloid fibrils that regulate gut and host physiological functions.[16]

Previously, we found that the specific microbiome *Proteus mirabilis* (*P. mirabilis*) induces brain dopaminergic neurodegeneration from the gut to the brain.[17] Choi et al. identified significantly increased *P. mirabilis* levels in the faeces of murine PD models and found neurodegeneration in the nigrostriatal pathway by neuroinflammation and α-syn aggregation, contributing to motor dysfunction when mice were gavaged with *P. mirabilis*. The authors also demonstrated that inoculation of *P. mirabilis* in the mouse intestine induced α-syn inclusions and the disruption of enteric neurones by inducing systemic inflammation. Mechanistic investigations into the pathological effects of *P. mirabilis*

have also been conducted. Based on a previous study, we focused on the specific virulence factors of *P. mirabilis* to elucidate their precise mechanisms.

In this study, we aimed to characterise the mechanisms underlying the pathological effects of *P. mirabilis*-induced neurodegeneration in the GI tract. We observed the aetiology of motor impairment and neuronal cell death in *P. mirabilis* as a α-syn pathology both in the intestine and in the brain. We then identified the specific bacterial virulence factor of *P. mirabilis* that induces PD pathology and revealed its mechanisms by evaluating molecular expressions that are related to autophagy pathways in intestinal cells.

Methods

Bacterial culture conditions

P. mirabilis, isolated in the previous study,[17] was cultured in 500 mL of GAM broth at 37 °C for 24 h (optical density, 1.2–1.5; colony-forming units, >5 × 10^8 CFU/mL) under anaerobic incubator (Don Whitley Scientific Ltd. (West Yorkshire, UK) and centrifuged at 7000 × *g* at 4 °C for 30 min. The collected cells were suspended in sterile saline for *in vitro* and *in vivo* experiments. Mutated *P. mirabilis* (ΔMrpA, ΔHpmA, and ΔUreC) were generated as previously described[18] and cultured in the same condition as the wild type of *P. mirabilis*.

Plasmid construction and expression in *E. coli*

Gene encoding the HpmA was amplified by polymerase chain reaction (PCR) from *P. mirabilis* genomic DNA using forward primer 5′-AAA AAA CAT ATG AAA TCA AAA AAC TTT AAA CTT TC-3′ and reverse primer 5′-AAA AAA CTC GAG CTA TTT TTC AGA AAT AGA TGC TTT TG-3'. Amplified HpmA gene was directly cloned to pGEM®-T easy vector (Promega, USA), referred to as pGEM-T HpmA. The integrity of all sequences was verified by DNA sequence analyses. Plasmid pGEM-T HpmA was digested completely with Nde I, and then partially with Xho I. Approximately 4.8 kb DNA fragment containing the whole HpmA gene was subcloned into pET15b (Novagen, USA) plasmids, resulting in pET15b-HpmA. The pET15b-HpmA plasmid was transformed into *E. coli* BL21 (DE3) cells. Protein expression was induced by the addition of 1 mM of IPTG and analysed by SDS-PAGE.

Ethics

All animal studies were conducted following the "Principles of Laboratory Animal Care" (NIH publication, 1996) and approved by the "Animal Care and Use Guidelines" of Kyung Hee University, Seoul, Korea (KHUASP(SE)-18-007 and 20–029).

Animals

Seven-week-old male C57BL/6 J mice were used. Mice were housed in cages (eight mice per group) at an optimal temperature and humidity (23 ± 1 °C and 60 ± 10%) for 7 days. Since the disease model induced by *P. mirabilis* was verified only in male mice, female mice were not used in this study. All the experiments were grouped based on weight. There is no evidence of a difference in the means and standard error of mice weights between groups. We conducted a stratified randomisation based on the mouse weight and analysed their differences using one-way analysis of variance (ANOVA; Experimental 1: $F(3, 28) = 0.8810$, $P = 0.4624$; Experiment 2: $F(3, 28) = 0.9632$, $P = 0.4233$; Experiment 3: $F(4, 35) = 0.9993$, $P = 0.4210$; Supplementary experiment 1: $F(3, 28) = 1.197$, $P = 0.3290$; Supplementary experiment 2: $F(3, 28) = 0.6845$, $P = 0.5690$), so that the mean weights were the same for the experimental groups.

Experiment 1: Thirty-two mice were used in experiment 1. This experiment aimed to verify whether pathological manifestations in the brain induced after the inoculation of *P. mirabilis* in the intestine. The mice were divided into four groups as follows: (1) Control-Vehicle (saline-treated plus phosphate-buffered saline (PBS)-treated group, n = 8), (2) Control-*P. mirabilis* (saline-treated plus *P. mirabilis*-treated group, n = 8), (3) ABX-Vehicle group (antibiotic-treated plus PBS-treated group, n = 8), and (4) ABX-*P. mirabilis* (antibiotic-treated plus *P. mirabilis*-treated group, n = 8). *P. mirabilis* was orally administered to the mice for 5 days (2 × 10^8 CFU/0.2 mL PBS per mouse). For antibiotic treatment, the mice were administered ciprofloxacin (40 mg/kg per mouse by oral gavage) for 3 days from the day after the end of the *P. mirabilis* treatment, based on a previous study.[19,20] An equal volume of PBS was orally administered to the PBS-treated group for 5 days. The mice were sacrificed on the 16th day after the last administration of the microbiota.

Experiment 2: Thirty-two mice were used in experiment 2. This experiment aimed to investigate whether pathological brain manifestations induced by *P. mirabilis* are mediated by the vagus nerve. The mice were divided into four groups as follows: (1) Sham-Vehicle (sham-operated plus PBS-treated group, n = 8), (2) Sham-*P. mirabilis* (sham-operated plus *P. mirabilis*-treated group, n = 8), (3) VGX-vehicle (vagotomised plus PBS-treated group, n = 8) and (4) VGX-*P. mirabilis* (vagotomised plus *P. mirabilis*-treated group, n = 8). Vagotomy was performed as detailed in a previous study.[17] Briefly, the mice were incised into the anterior neck skin to localise the right vagus nerve bundle. The vagus nerve was carefully cut and the skin was closed with a surgical suture. The vagal bundles of sham-operated mice were exposed, but the vagus nerve was not cut. Seven days after surgery, the mice were gavaged with *P. mirabilis* for 5 days (2 × 10^8 CFU/0.2 mL PBS per mouse). An equal volume of PBS was orally administered to the PBS-treated group for 5 days. The

mice were sacrificed on the 16th day after the last administration of the microbiota.

Experiment 3: Forty mice were used in experiment 3. This experiment aimed to identify the pathological virulence factors of *P. mirabilis*. The mice were divided into five groups as follows: (1) Normal (PBS-treated group, n = 8), (2) *P. mirabilis*^{WT} (*P. mirabilis*^{WT}-treated group, n = 8), (3) *P. mirabilis*$^{\Delta MrpA}$ (*P. mirabilis*$^{\Delta MrpA}$-treated group, n = 8), (4) *P. mirabilis*$^{\Delta HpmA}$ (*P. mirabilis*$^{\Delta HpmA}$-treated group, n = 8) and (5) *P. mirabilis*$^{\Delta UreC}$ (*P. mirabilis*$^{\Delta UreC}$-treated group, n = 8). Microbiota were orally administered to the mice for 5 days (2×10^8 CFU/0.2 mL PBS per mouse). The Normal was orally administered an equal volume of PBS for 5 days. The mice were sacrificed on the 16th day after the last administration of the microbiota.

Supplementary experiment 1: Thirty-two mice were used in the supplementary experiment 1. The experiment aimed to compare the pathological effects of microbiota included in *Proteus* genus. Mice were randomly divided into four groups as follows; (1) Normal group (PBS-treated group, n = 8), (2) *P. mirabilis* group (*P. mirabilis*-treated group, n = 8), (3) *P. cibarius* group (*P. cibarius*-treated group, n = 8) and (4) *P. vulgaris* group (*P. vulgaris*-treated group, n = 8). Microbiota was administered to mice for 5 days (2×10^8 CFU/0.2 mL PBS per mouse). The normal group was orally administered an equal volume of PBS for 5 days. Mice were sacrificed on the 16th day after the last administration of microbiota.

Supplementary experiment 2: Thirty-two mice were used in the supplementary experiment 2. The experiment aimed to confirm the pathological effects of Haemolysin A derived from *P. mirabilis*. Mice were randomly divided into four groups as follows; (1) Normal (PBS-treated group, n = 8), (2) *P. mirabilis* ^{WT} (*P. mirabilis* ^{WT}-treated group, n = 8), (3) *E. coli*^{WT} (*E. coli*^{WT}-treated group, n = 8) and (4) *E. coli*$^{HpmA+/+}$ (*E. coli*$^{HpmA+/+}$-treated group, n = 8). Microbiota was orally administered to mice for 5 days (2×10^8 CFU/0.2 mL PBS per mouse). The normal group was orally administered an equal volume of PBS for 5 days. Mice were sacrificed on the 16th day after the last administration of microbiota.

Motor function assessment

Motor function was assessed as described in previous studies.[17] The rotarod test was trained for 2 days. All experiments were conducted between 10 am and 8 pm to avoid diurnal variations. The rest of the time was spent maintaining the experimental conditions.

Open-field test- The mice were tested in a box (40 × 25 × 18 cm) for 30-min using a computerised automatic analysis system. The data were used to calculate the total distance traveled.

Rotarod test- The rotarod unit included a rotating spindle (7.3 cm diameter, Rotarod apparatus for mouse, Jeung Do Bio&Plant, South Korea). The day before examination, the mice were trained on the rods. The rotarod test was performed at rotation speeds varying from 8 to 10 rpm. During the test session, the rotational speed was in the range 12–16 rpm. The duration for which each mouse remained on the rotating rod until falling (latency time) was recorded using a built-in sensor.

Pole test- A 0.5 m long pole made by custom order, was placed in the cage. On the test assessment, mice were placed on the top of the pole with head-up and timed from the beginning when mice were head-down to the ending when all limbs were placed on the cage. Latency time was cross-checking by two independent experimenters. The landing time was averaged over three trials. Pole test was conducted between 10 am and 8 pm to avoid diurnal variations. Rest time was spent to maintain the experimental conditions of mice.

Cells

The STC-1 cell line (CVCL_J405, Cat. No. CRL-3254, ATCC) was grown at 37 °C in 5% CO_2 in DMEM medium (Corning), supplemented with 10% heat-inactivated foetal bovine serum, 100 U/mL penicillin, and 100 μg/mL streptomycin. Mycoplasma testing was confirmed as negative upon receipt of the cells and before conducting the experiment, and they were used in the experiment within one month thereafter.

The experiments were performed 48 h after STC-1 cell seeding. The cell density of each plate was 0.8×10^6 cells/plate for 60-mm dishes. Cells were treated with HpmA (0.01, 0.1, 1, or 10 μM) or 10 nM rapamycin (RAPA) in low-serum media for 48 h and harvested for protein extraction.

Western blot

To prepare proteins for western or dot blotting, harvested cell pellets or 15 mg of tissue from the distal colon were lysed in ice-cold RIPA buffer containing a protease/phosphatase inhibitor cocktail. Protein extract was separated on an 10–12% polyacrylamide gel and transferred to a PVDF membrane (Millipore). Membranes were blocked with 5% skim milk in Tris-buffered saline (TBS) and incubated with primary antibodies overnight at 4 °C in 1% skim milk in TBS-Tween (TBS-T): anti-α-syn (AB_398107, 1:5000), anti-A11 (AB_2536236, 1:1000), anti-cytochrome C (AB_627385, 1:2000), anti-Bcl 2 (AB_2243455, 1:500), anti-Bax (AB_306191, 1:500), anti-phosphor-mTOR (AB_330970, 1:1000), anti-total mTOR (AB_330978, 1:1000), anti-LC3B (AB_881433, 1:1000), anti-Beclin1 (AB_490837, 1:1000) and anti-β-actin (AB_2714189, 1:3000).

To prepare proteins for western blotting of α-syn, a harvested cell pellet or 15 mg of tissue from the distal colon was lysed in PBS containing 10% Triton X-100 and protease/phosphatase inhibitor cocktail. After incubation on ice for 20 min, the supernatant was used as the soluble fraction of monomeric α-syn. Pellets were

lysed in 50 mM Tris–HCl containing 2% SDS and protease/phosphatase inhibitor cocktail. Twenty microgram of protein extract were separated on 12% polyacrylamide gel and transferred to a PVDF membrane (Millipore). The membranes were blocked with 5% skim milk in TBS and incubated overnight at 4 °C in 1% skim milk in TBS-T containing anti-α-syn (AB_398107, 1:1000) and anti-β-actin (AB_2714189, 1:3000) antibodies.

The membranes were washed in TBS-T and incubated in 1% skim milk in TBS-T with goat anti-mouse HRP or goat anti-rabbit HRP secondary antibody (1:3000). The membranes were washed and imaged using Image Lab software (Bio-Rad, CA, USA).

Histology and immunofluorescence

Free-floating brain sections were rinsed with PBS and treated with 1% hydrogen peroxide. Then they were incubated overnight with a rabbit anti-TH antibody (AB_390204, 1:1000) in 0.3% Triton X-100 in PBS and subsequently incubated with a biotinylated anti-rabbit IgG antibody (1:200), followed by incubation in ABC solution. The colour was developed with DAB. The brain tissue sections were quantified by counting the number of TH-immunopositive neurones in the Substantia nigra pars compacta (SNpc) at × 200 magnification and measuring the optical density of TH-positive fibres in the ST at × 40 magnification using the Image J software (Bethesda, MD, USA).

For proteinase K treatment, ST and SN tissues were reacted with 10 μg/mL proteinase K in PBS before the 1% hydrogen peroxide reaction. Tissues were incubated overnight with mouse anti-α-syn (AB_398107, 1:1000) antibody in normal goat serum. They were then incubated with biotinylated anti-mouse IgG (1:200), followed by incubation in the ABC solution. The colour was developed with DAB. Quantification of the brain tissue sections was performed by measuring the optical density of α-syn -positive signals in the ST at × 40 magnification and SN at × 100 magnification. Images were captured using an optical light microscope (Olympus Microscope System BX51; Olympus, Tokyo, Japan).

For immunofluorescence, the brain tissues were rinsed in PBS and incubated overnight with goat or rabbit anti-TH (1:1000), rabbit anti-aggregated α-syn (AB_2714215, 1:1000), or mouse anti-Iba-1 (AB_2224402, 1:1000) antibodies. They were then incubated with goat anti-rabbit DyLight 594 (AB_2336413, 1:500), chicken anti-goat Alexa 488 (AB_2535870, 1:500), or goat anti-mouse Alexa 488 (AB_2534073, 1:500). Images were captured under a confocal microscopy at × 200 magnification ([K1-Fluo]; Nanoscope Systems, Daejeon, Korea).

For immunofluorescence of STC-1 cells, the fixed cells were rinsed in PBS and incubated overnight with rabbit anti-LC3 (AB_881433, 1:1000) and mouse anti-phospho α-syn (AB_2819037, 1:5000) antibodies. They were then incubated with goat anti-rabbit Alexa 488 (AB_143165, 1:500), or goat anti-mouse Alexa 594 (AB_2534073, 1:500). Images were captured under a confocal microscopy at × 1200 magnification [K1-Fluo].

Quantitative real-time polymerase chain reaction (qPCR)

Cells or tissues were dissected and prepared to extract total RNA using an RNeasy Plus Mini Kit (Qiagen, Hilden, Germany), according to the manufacturer's instructions. cDNA synthesis from RNA samples was performed using TOPscript™ RT DryMIX (Enzynomics, Daejeon, Republic of Korea). cDNA was subjected to qRT-PCR using TOP real™ qPCR 2X PreMIX (SYBR Green; Enzynomics, Daejeon, Republic of Korea) and a CFX Connect real-time PCR system (Bio-Rad Laboratories, Hercules, CA, United States). Primers, synthesized at Cosmo Genetech (Seoul, Republic of Korea), were shown in Supplementary Table S1. As a loading control, GAPDH or 16 S was used for normalisation of the biomarker expression.

Calcein-leakage assay

The calcein-leakage assay method has been reported previously.[21]

Calcein-roaded Liposome- Briefly, the lipids (1-Palmitoyl-2-oleoyl-phosphatidylcholine; POPC, 1-Palmitoyl-2-oleoyl-phosphatidylglycerol; POPG, Cholesterol) were dissolved at a concentration of 10 mM using $CHCl_3$ at 4 °C. Subsequently, the lipid components (POPC, POPG, and Cholesterol) were mixed in appropriate proportions (60 mol%:30 mol%:10 mol % = POPC:POPG:Cholesterol). To obtain the lipid film, $CHCl_3$ was gently removed using Argon gas and desiccated for 1 h. The prepared lipid film was added to aqueous buffer A (20 mM Na,K-phosphate, 0.8 mM EGTA, 150 mM NaCl, 10 mM calcein disodium salt, pH 7.2) and mixed by vortexing. The colour was a cloudy green. To form uniform liposomes, the lipid mixture was extruded using a mini-extruder (cat. No: NC9273238, Avanti Polar Lipids. Inc., Japan) with a polycarbonate filter (pore size: 100 nm). To remove unloaded calcein, dialysis was performed for 2 days in buffer A.

Prepared Dodecylphosphocholine (DPC) suspension- Briefly, DPC suspension was made in aqueous buffer B (20 mM Na,K-phosphate, 0.8 mM EGTA, 150 mM NaCl, 30 mM myoinositol, pH 7.2) at a concentration of 8 mM. Then, α-syn, HpmA, and α-syn + HpmA were dissolved at 200 μM, respectively.

Measurement of released calcein- Before fusion between DPC and calcein-roaded liposome, DPC was incubated for 4 h at 4 °C. The DPC suspension

containing the tested samples was treated with calcein-loaded liposomes (time point: 50 s). The lipid concentration was 20 μM. The measurements were performed using a fluorospectrometer (SHIMADZU Corp. RF-6000, Japan).

Thioflavin T (Th-T) assay

HpmA and α-syn were diluted in KPi to obtain accurate concentrations. Samples were incubated in 96-well, black, flat-bottom plates at 37 °C with Th T. Th T fluorescence was monitored every 15 min for 24 h with a FLUOstar omega plate reader (excitation: 470 nm; emission: 520 nm). Thirty seconds of shaking of plate prior to every measurement was conducted.

Statistics

The primary outcome of animal experiments was the behavioural abnormalities, and sample size was calculated with 90% statistical power and a significance level of 0.05 assuming the results of open-field test using InVivoStat as described previously.[22] Then, we also set the exclusion criteria as the weight loss of mouse exceeding 15% with the baseline (the day before *P. mirabilis* administration) until the humane endpoint. No mice were excluded from the study. Experimenters who could identify groups and mice performed mouse administration and the behavioural and tissue experiments. However, the study was conducted and statistical analyses was performed by an experimenter who was blinded to the information of each group. For example, in the case of the behaviour test, blinding analyses were performed by recording, and the tissue test results were also analysed by an experimenter who had restricted access to the group information.

To statistically analyse the data, we first performed the Shapiro–Wilk test to evaluate normality. Multiple group comparisons were made using one-way ANOVA followed by Dunnett's multiple comparison test (Fig. 1, Fig. 2, Fig. 3, Fig. 4, Fig. 5). Two-tailed unpaired t-tests were conducted as shown in Fig. 6. In Fig. 7, statistical analysis was utilised by one-way ANOVA followed by Dunnett's multiple comparison test. $P < 0.05$ was considered statistically significant. All data are expressed as the mean ± standard error of the mean (SEM). Statistical analyses were performed using GraphPad Prism software (GraphPad Software, La Jolla, CA, USA).

Role of funders

This study was supported by the Medical Research Centre Program through the National Research Foundation of Korea funded by the Ministry of Science and ICT (NRF-2017R1A5A2014768). The funding body did not play a role in the study design, data collection, data analyses and interpretation, or writing of the manuscript.

Results

P. mirabilis inoculation in the mouse intestine induces PD-like brain pathological degeneration

First, we confirmed whether *P. mirabilis* could affect PD pathology in the gut of conventional mice (Fig. 1). *P. mirabilis*-treated mice showed significant motor dysfunction compared with vehicle-treated mouse (Fig. 1b and c and Fig. 2b and c) as well as neurodegeneration in the nigrostriatal pathway (Fig. 1d–f and Fig. 2d–f). *P. mirabilis*-treated mice had α-syn aggregation in the SNpc region, while vehicle-treated mice did not (Fig. 1g and h and Fig. 2g, h). We also examined the possibility of the pathogenesis of PD induced by *Proteus* at the genus level. We used three species: *P. vulgaris*, *P. cibarius*, and *P. mirabilis* (Supplementary Fig. S1a). The results showed that only *P. mirabilis* induced motor deficits (Supplementary Fig. S1b and d) as well as brain damage including dopaminergic neuronal death, neuroinflammation, and α-syn aggregation (Supplementary Fig. S1e–k).

To establish whether inoculation with *P. mirabilis* is critical for the pathogenesis of PD, we depleted colonic *P. mirabilis* in mice that were treated with antibiotic for 3 days after *P. mirabilis* administration (Fig. 1a). Without antibiotic administration, *P. mirabilis* treatment impaired motor function compared with vehicle treatment (locomotive track length (mean ± SEM, pixels): Control-Vehicle group = 29657.00 ± 977.20, Con-*P. mirabilis* group = 26016.00 ± 726.00; latency time on rod (mean ± SEM, sec): Control-Vehicle group = 128.60 ± 16.80, Con-*P. mirabilis* group = 68.75 ± 9.82) in the open-field test ($F(3, 28) = 3.695$, $P = 0.0233$, one-way ANOVA measures; $P = 0.0161$, Dunnett's posthoc test) and the rotarod test ($F(3, 28) = 2.967$, $P = 0.0490$, one-way ANOVA measures; $P = 0.0392$, Dunnett's posthoc test), respectively; however, antibiotics-treated mice after gavage with *P. mirabilis* recovered *P. mirabilis*-induced motor manifestations (locomotive track length (mean ± SEM, pixels): $P = 0.0456$, Dunnett's posthoc test, ABX-*P. mirabilis* group = 29953.00 ± 1509.00; latency time on rotarod (mean ± SEM, sec): $P = 0.0370$, Dunnett's posthoc test, ABX-*P. mirabilis* group = 130.40 ± 19.26). Antibiotic treatment did not affect motor functions in vehicle-treated mice (locomotive track length: $P = 0.8022$, Dunnett's posthoc test, ABX-Vehicle group = 30809.00 ± 1048.00 pixels; latency time on rod: $P = 0.7993$, Dunnett's posthoc test, ABX-Vehicle group = 111.10 ± 18.91 s; Fig. 1b and c). The dopaminergic neurones that were disrupted in the *P. mirabilis*-inoculated mouse SNpc (mean ± SEM, cells/mm^3; Control-Vehicle group = 3761.00 ± 566.10, Con-*P. mirabilis* group = 1991.00 ± 264.10) were significantly reversed when treated with antibiotic (mean ± SEM, cells/mm^3; ABX-Vehicle group = 3025.00 ± 205.40, ABX-*P. mirabilis* group = 3287.00 ± 432.80; $F(3, 28) = 3.459$, $P = 0.0398$, one-way ANOVA measures;

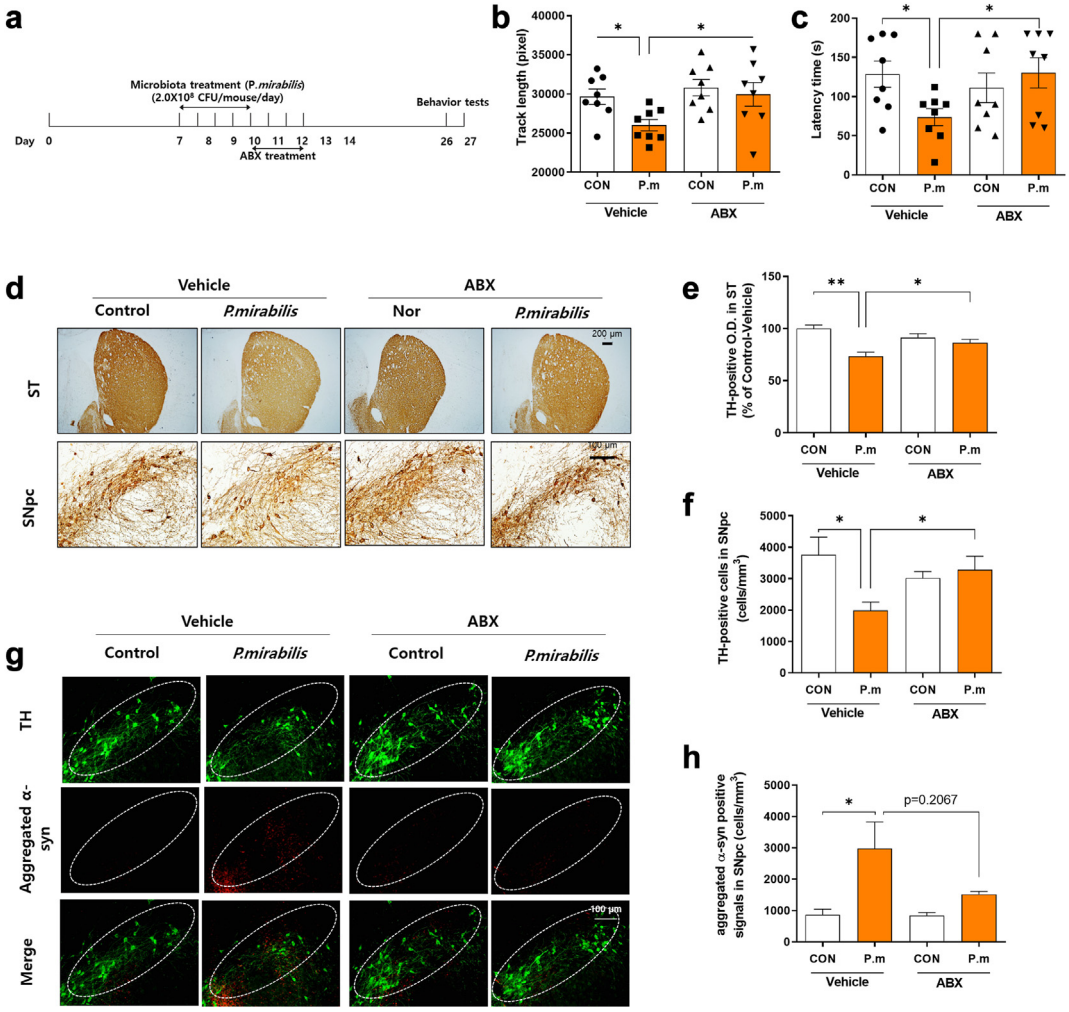

***Fig. 1: P. mirabilis* inoculation in the mouse intestine induces PD.** (a–h) Mice were gavaged with *P. mirabilis* with antibiotics (N = 8 per group). (a) Schematic diagram of the treatment schedule and timeline for behavioural tests. (b and c) Behavioural function investigated with open-field test and rotarod test. (d–f) Tyrosine hydroxylase (TH)-positive optical density or cells in the striatum (40 × magnification, scale bar = 200 μm; N = 8 per group) or substantia nigra pars compacta (SNpc; 200 × magnification, scale bar = 100 μm; N = 8 per group). (g and h) Analysis of aggregated α-syn-positive signals (Red) in the mouse SNpc (200 × magnification, scale bar = 100 μm; N = 8 per group). White line indicated the region of the SNpc that include TH signals with Green. Data are presented as mean with error bars, SEM. Statistical analyses were performed by one-way ANOVA with Dunnett's multiple comparison test. Statistical significances were indicated by * $P < 0.05$ and ** $P < 0.01$. This experiment was repeated twice. Group information: (1) Vehicle + PBS: mice treated with vehicle plus PBS orally; (2) Vehicle + P.m: mice treated with vehicle plus *P. mirabilis* orally; (3) ABX + PBS: mice treated with antibiotics plus PBS orally; (4) ABX + P.m: mice treated with antibiotics plus *P. mirabilis* orally.

P value compared to Con-Vehicle group: Con-*P. mirabilis*, P = 0.0154; ABX-Vehicle, P = 0.4060, Dunnett's posthoc test; P value compared to Con-*P. mirabilis* group: ABX-*P. mirabilis*, P = 0.0453, Dunnett's posthoc test; Fig. 1d and f). Similarly, loss of striatal dopaminergic fibres in *P. mirabilis*-treated mice were significantly increased in the antibiotic group (mean ± SEM, % of Control-Vehicle group; Control-Vehicle group = 100.00 ± 3.28, Con-*P. mirabilis* group = 73.43 ± 3.89, ABX-Vehicle group = 91.24 ± 3.84, ABX-*P. mirabilis* group = 86.26 ± 3.39; F (3, 28) = 8.333, P = 0.0024, one-way ANOVA measures; P value compared to Con-Vehicle group: Con-*P. mirabilis*, P = 0.0011; ABX-Vehicle, P = 0.3288, Dunnett's posthoc test; P value compared to Con- *P. mirabilis* group: ABX-*P. mirabilis*, P = 0.0440, Dunnett's posthoc test; Fig. 1d and e). In addition, *P. mirabilis* treatment increased brain α-syn aggregation compared to the vehicle-treated mice; however, antibiotics administration inhibited brain

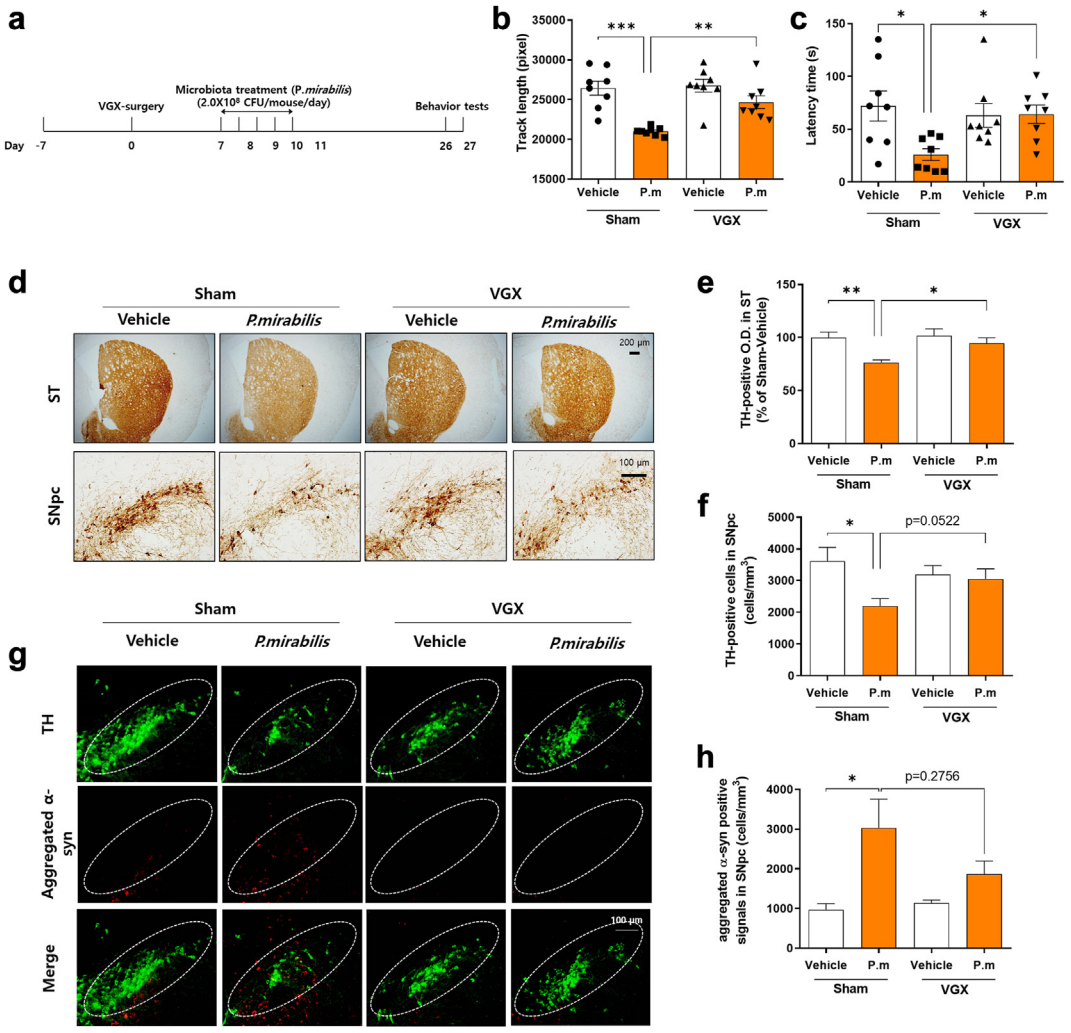

***Fig. 2: P. mirabilis* inoculation in the mouse intestine propagates α-syn from the gut to the brain.** (a–h) Mice were gavaged with *P. mirabilis* after vagotomy. (a) Schematic diagram of the treatment schedule and timeline for behavioural tests (N = 8 per group). (b and c) Behavioural function investigated with open-field test and rotarod test. (d–f) Tyrosine hydroxylase (TH)-positive optical density or cells in the striatum (40 × magnification, scale bar = 200 μm; N = 8 per group) or substantia nigra pars compacta (SNpc; 200 × magnification, scale bar = 100 μm; N = 8 per group). (g and h) Analysis of aggregated α-syn-positive signals (Red) in the mouse SNpc (200 × magnification, scale bar = 100 μm; N = 8 per group). White lines indicate the region of the SNpc that include TH signals with Green. Data are presented as mean with error bars, SEM. Statistical analyses were performed by one-way ANOVA with Dunnett's multiple comparison test. Statistical significances were indicated by * P < 0.05, ** P < 0.01 and *** P < 0.001. This experiment was repeated twice. Group information: (1) Sham + PBS: Sham-mice treated with PBS orally; (2) Sham + P.m: Sham-mice treated with *P. mirabilis* orally; (3) VGX + PBS: Vagotomised mice treated with PBS orally; (4) VGX + P.m: Vagotomised mice treated with *P. mirabilis* orally.

α-syn aggregation by half in mice that were gavaged with *P. mirabilis* (mean ± SEM, cells/mm^3; Control-Vehicle group = 865.90 ± 182.10, Con-*P. mirabilis* group = 2980.00 ± 849.30, ABX-Vehicle group = 838.40 ± 100.10, ABX-*P. mirabilis* group = 1523.00 ± 88.52; F (3, 28) = 3.636, P = 0.04210, one-way ANOVA measures; P value compared to Con-Vehicle group: Con-*P. mirabilis*, P = 0.0318; ABX-Vehicle, P > 0.9999, Dunnett's posthoc test; P value compared to Con- *P. mirabilis* group: ABX-*P. mirabilis*, P = 0.2067, Dunnett's posthoc test; Fig. 1g and h).

P. mirabilis induces PD via propagation of α-syn from the gut to the brain

To determine the possible pathway of the pathogenesis of PD induced by *P. mirabilis* from the gut to the brain, we performed a vagotomy before administering *P. mirabilis* to the mice (Fig. 2a). Vagotomised-mice

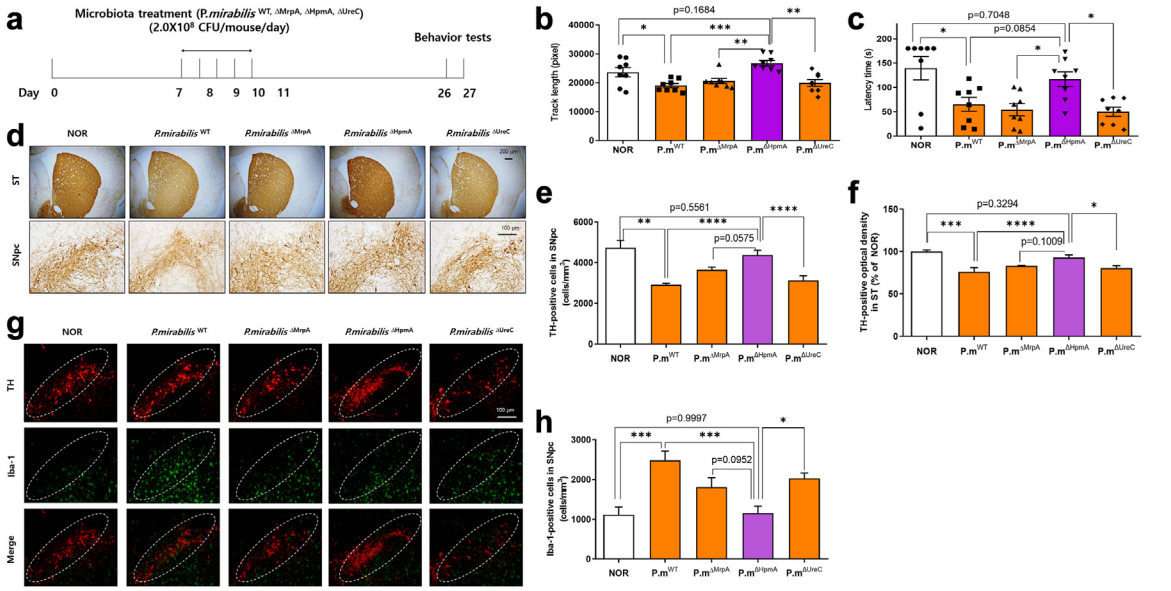

Fig. 3: **Haemolysin A-mutated *P. mirabilis* does not induce the pathological manifestations in the mouse**. (a) Schematic diagram of the treatment schedule and timeline for behavioural tests (N = 8 per group). (b and c) Behavioural function investigated with open-field test and rotarod test. (d–f) Tyrosine hydroxylase (TH)-positive optical density or cells in the striatum (40 × magnification, scale bar = 200 μm; N = 8 per group) or substantia nigra pars compacta (SNpc; 200 × magnification, scale bar = 100 μm; N = 8 per group). (g and h) Analysis of activated microglial cells (Green) in the mouse SNpc (200 × magnification, scale bar = 100 μm; N = 8 per group). White line indicated the region of the SNpc which included TH signals with Red. Data are presented as mean with error bars, SEM. Statistical analyses were performed by one-way ANOVA with Dunnett's multiple comparison test. Statistical significances were indicated by * P < 0.05, ** P < 0.01, *** P < 0.001 and **** P < 0.0001. This experiment was repeated three times. Group information: (1) PBS: mice treated with PBS orally; (2) P.m^{WT}: mice treated with wild type of *P. mirabilis* orally; (3) P.m$^{\Delta mrpA}$: mice treated with MrpA deleted *P. mirabilis* orally; (4) P.m$^{\Delta HpmA}$: mice treated with HpmA deleted *P. mirabilis* orally. (5) P.m$^{\Delta UreC}$: mice treated with UreC deleted *P. mirabilis* orally.

were significantly protected from *P. mirabilis*-induced deficits in motor functions in the open-field test (locomotive track length (mean ± SEM, pixels): Sham-Vehicle group = 26447.00 ± 885.70, Sham-*P. mirabilis* group = 21003.00 ± 179.20, VGX-Vehicle group = 26758.00 ± 817.70, VGX-*P. mirabilis* group = 24665.00 ± 807.80; F (3, 28) = 13.07, P < 0.0001, one-way ANOVA measures; P value compared to Sham-Vehicle group: Sham-*P. mirabilis*, P < 0.0001, Dunnett's posthoc test; P value compared to Sham-*P. mirabilis* group: VGX-*P. mirabilis*, P = 0.0039, Dunnett's posthoc test) and the rotarod test (latency time on rod (mean ± SEM, sec): Sham-Vehicle group = 72.00 ± 14.35, Sham-*P. mirabilis* group = 26.00 ± 5.61, VGX-Vehicle group = 63.11 ± 11.16, VGX-*P. mirabilis* group = 64.25 ± 8.68; F (3, 28) = 3.886, P = 0.0193, one-way ANOVA measures; P value compared to Sham-Vehicle group: Sham-*P. mirabilis*, P = 0.0116, Dunnett's posthoc test; P value compared to Sham-*P. mirabilis* group: VGX-*P. mirabilis*, P = 0.00397, Dunnett's posthoc test). In addition, vagotomy did not affect motor function in normal mice (P value compared to Sham-Vehicle group in open-field test: VGX-Vehicle, P = 0.9814; P value compared to Sham-Vehicle group in rotarod test: VGX-Vehicle, P = 0.8786, Dunnett's posthoc test; Fig. 2b and c). Histological alterations in the brain that were induced by *P. mirabilis* were protected when vagotomies were performed in the mice. We found that vagus ganglionectomy could protect against *P. mirabilis*-induced dopaminergic neuronal cells (mean ± SEM, cells/mm^3; Sham-Vehicle group = 3617.00 ± 434.70, Sham-*P. mirabilis* group = 2196.00 ± 233.40, VGX-Vehicle group = 3189.00 ± 287.00, VGX-*P. mirabilis* group = 3048.00 ± 324.2; F (3, 28) = 3.160, P = 0.0422, one-way ANOVA measures; P value compared to Sham-Vehicle group: Sham-*P. mirabilis*, P = 0.0157; VGX-Vehicle, P = 0.6778, Dunnett's posthoc test; P value compared to Sham-*P. mirabilis* group: VGX-*P. mirabilis*, P = 0.0522, Dunnett's posthoc test) and fibres (mean ± SEM, % of Sham-Vehicle group; Sham-Vehicle group = 100.00 ± 5.20, Sham-*P. mirabilis* group = 76.44 ± 2.40, VGX-Vehicle group = 101.70 ± 6.52, VGX-*P. mirabilis* group = 94.67 ± 5.13; F (3, 28) = 5.274, P = 0.0052, one-way ANOVA measures; P value compared to Sham-Vehicle group: Sham-*P. mirabilis*, P = 0.0072; VGX-Vehicle, P = 0.9901, Dunnett's posthoc test; P value compared to Sham-*P. mirabilis* group: VGX-

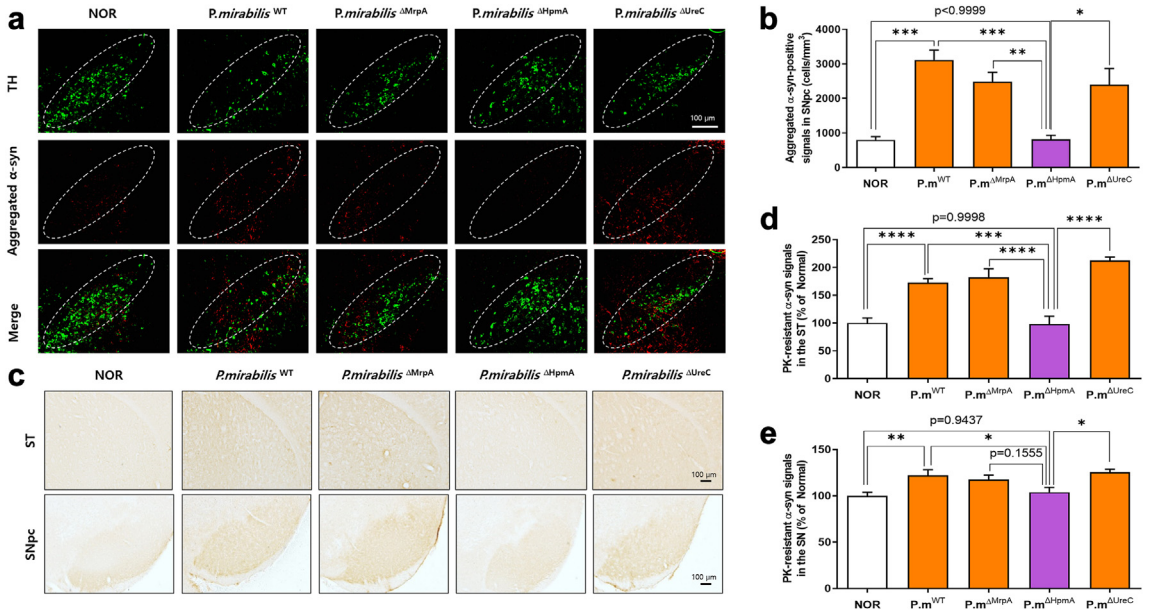

Fig. 4: **Haemolysin A-mutated *P. mirabilis* does not induce the aggregation of α-syn in the mouse brain**. (a and b) Analysis of aggregated α-syn-positive signals (Red) in the mouse substantia nigra pars compacta (SNpc; 200 × magnification, scale bar = 100 μm; N = 8 per group). White lines indicate the region of the SNpc that include TH signals with Green. (c–e) Proteinase K-resistant α-syn-positive optical density in the mouse striatum or SNpc (100 × magnification, scale bar = 100 μm; N = 8 per group). Data are presented as mean with error bars, SEM. Statistical analyses were performed by one-way ANOVA with Dunnett's multiple comparison test. Statistical significances were indicated by * P < 0.05, ** P < 0.01, *** P < 0.001 and **** P < 0.0001. This experiment was repeated three times. Group information: (1) PBS: mice treated with PBS orally; (2) P.m^{WT}: mice treated with wild type of *P. mirabilis* orally; (3) P.m$^{\Delta mrpA}$: mice treated with MrpA deleted *P. mirabilis* orally; (4) P.m$^{\Delta HpmA}$: mice treated with HpmA deleted *P. mirabilis* orally. (5) P.m$^{\Delta UreC}$: mice treated with UreC deleted *P. mirabilis* orally.

P. mirabilis, P = 0.0425, Dunnett's posthoc test) degeneration at a normal level (Fig. 2d–f). The α-syn aggregation in the mouse SNpc was increased more than 3-fold by *P. mirabilis*. Increased α-syn was reduced by 40% in the vagus nerve resected mouse SNpc (mean ± SEM, cells/mm^3; Sham-Vehicle group = 968.40 ± 155.90, Sham-*P. mirabilis* group = 3032.00 ± 723.60, VGX-Vehicle group = 1143.00 ± 70.81, VGX-*P. mirabilis* group = 1873.00 ± 327.2; F (3, 28) = 4.069, P = 0.0267, one-way ANOVA measures; P value compared to Sham-Vehicle group: Sham-*P. mirabilis*, P = 0.0175; VGX-Vehicle, P = 0.9903, Dunnett's posthoc test; P value compared to Sham-*P. mirabilis* group: VGX-*P. mirabilis*, P = 0.2756, Dunnett's posthoc test; Fig. 2g and h). Collectively, these findings confirmed that the pathology of *P. mirabilis*-induced brain degeneration may be mediated by the vagus pathway.

P. mirabilis-induced PD like motor impairment and brain neuronal death are related to haemolysin A, HpmA

To elucidate the key factors in the *P. mirabilis*-induced pathophysiology of PD, gene-mutant *P. mirabilis* was used for further study. Several virulence factors derived from *P. mirabilis*, such as fimbria (MrpA), haemolysin A (HpmA), and urease (UreC) are essential elements of intestinal disruption, inflammation, and Crohn's.[18,23] To investigate whether gene-depleted *P. mirabilis* (ΔMrpA, ΔHpmA, or ΔUreC) could induce bacterial-induced PD phenotypes, mice were gavaged with these factors (Fig. 3a). Surprisingly, the mice that were treated with HpmA-deleted *P. mirabilis* showed similar motor functions as normal mice (locomotive track length (mean ± SEM, pixels): Normal group = 23652.00 ± 1632.00, *P. mirabilis*^{WT} group = 19002.00 ± 179.20, *P. mirabilis*$^{\Delta MrpA}$ group = 20604.00 ± 889.00, *P. mirabilis*$^{\Delta HpmA}$ group = 26787.00 ± 937.70, *P. mirabilis*$^{\Delta UreC}$ group = 19947.00 ± 1183.00; F (4, 35) = 8.132, P < 0.0001, one-way ANOVA measures; P value compared to Normal group: *P. mirabilis*^{WT}, P = 0.0203, *P. mirabilis*$^{\Delta HpmA}$, P = 0.1684, Dunnett's posthoc test. Latency time on rod (mean ± SEM, sec): Normal group = 139.50 ± 24.14, *P. mirabilis*^{WT} group = 77.88 ± 16.82, *P. mirabilis*$^{\Delta MrpA}$ group = 57.88 ± 14.73, *P. mirabilis*$^{\Delta HpmA}$ group = 114.40 ± 16.24, *P. mirabilis*$^{\Delta UreC}$ group = 49.88 ± 9.46; F (4, 35) = 6.573, P = 0.0005, one-way ANOVA measures; P value compared to Normal group: *P. mirabilis*^{WT}, P = 0.0074, *P. mirabilis*$^{\Delta HpmA}$, P = 0.7048; Dunnett's posthoc test), whereas mice that

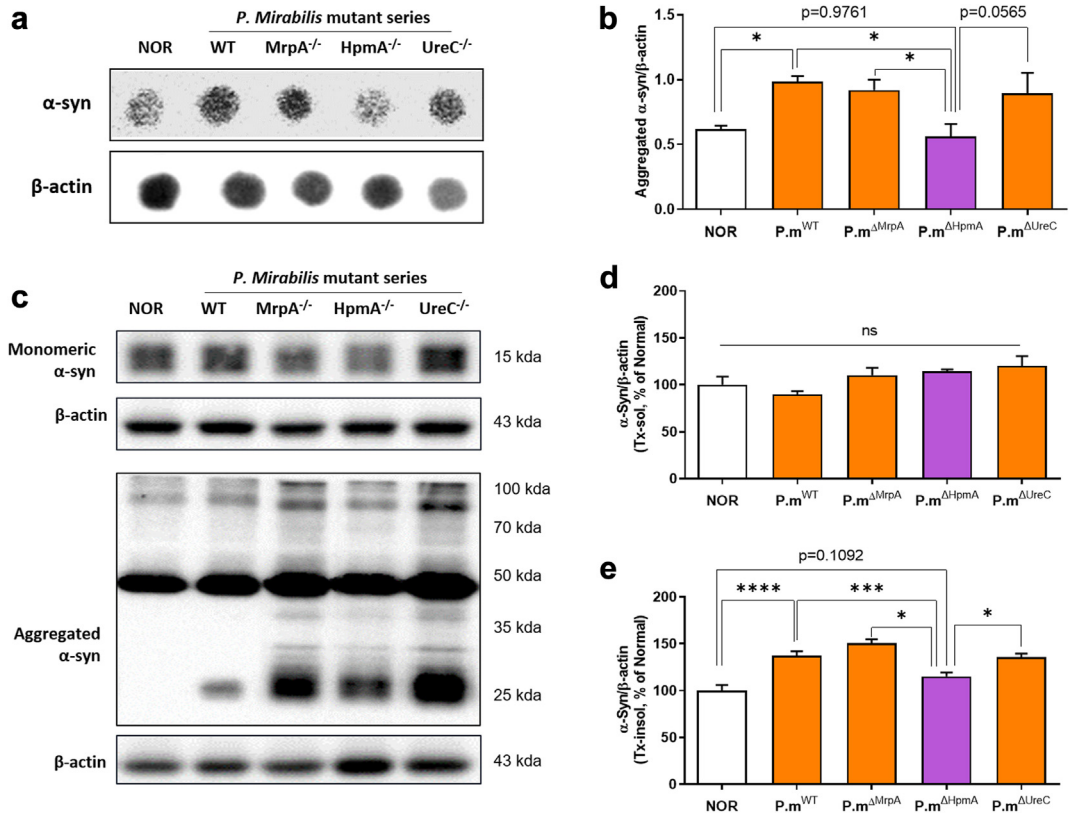

Fig. 5: **Haemolysin A-mutated *P. mirabilis* does not induce the α-syn aggregation in the mouse colon**. (a and b) Representative analysis of dot blot for the expression of aggregated α-syn in the mouse colon (left). The ratio of each dot density to that of β-actin was calculated and the relative expression levels were normalised by the normal group (Right, N = 8 per group). (c) Representative Western blot analysis for the expression of α-syn in the mouse colon (N = 8 per group). Proteins were fractionated by 10% Triton X-100 contained PBS. Soluble fraction was used for monomeric α-syn (upper) and the insoluble fraction was used for aggregated α-syn (bottom). (d and e) The ratio of each band density to that of β-actin was calculated and the relative expression levels were normalised by the normal group. (d) Expression of Triton X-100-soluble α-syn in the mouse colon (N = 8 per group). (e) Expression of Triton X-100-soluble α-syn in the mouse colon. Data are presented as mean with error bars, SEM. Statistical analyses were performed by one-way ANOVA with Dunnett's multiple comparison test. Statistical significances were indicated by * P < 0.05, *** P < 0.001 and **** P < 0.0001. This experiment was repeated three times. Group information: (1) PBS: mice treated with PBS orally; (2) P.m^{WT}: mice treated with wild type of *P. mirabilis* orally; (3) P.m$^{\Delta mrpA}$: mice treated with MrpA deleted *P. mirabilis* orally; (4) P.m$^{\Delta HpmA}$: mice treated with HpmA deleted *P. mirabilis* orally. (5) P.m$^{\Delta UreC}$: mice treated with UreC deleted *P. mirabilis* orally.

were treated with other gene-deleted *P. mirabilis* manifested motor dysfunctions similar to those that were treated with wild-type. In the open-field test, moving distance was reduced to approximately 80% in the mice that were treated with mutated *P. mirabilis*, except for those that were administered HpmA-deleted *P. mirabilis* (P value compared to *P. mirabilis*$^{\Delta HpmA}$ group: *P. mirabilis*^{WT}, P = 0.0002; *P. mirabilis*$^{\Delta MrpA}$, P = 0.0035; *P. mirabilis*$^{\Delta UreC}$, P = 0.0011, Dunnett's posthoc test). In addition, mice that were administered strains other than HpmA-mutated *P. mirabilis* showed reduced exercise capacity by half compared to normal mice in the rotarod test (P value compared to *P. mirabilis*$^{\Delta HpmA}$ group: *P. mirabilis*^{WT}, P = 0.0854; *P. mirabilis*$^{\Delta MrpA}$, P = 0.0278; *P. mirabilis*$^{\Delta UreC}$, P = 0.0174, Dunnett's posthoc test; Fig. 3b and c).

In the mouse brain, TH-positive signals decreased with intestinal inoculation of *P. mirabilis* including *P. mirabilis*$^{\Delta MrpA}$ and *P. mirabilis*$^{\Delta UreC}$. The striatal dopaminergic fibres were decreased by *P. mirabilis*-treated mice excluding *P. mirabilis*$^{\Delta HpmA}$ (mean ± SEM, % of Normal group; Normal group = 100.00 ± 1.79, *P. mirabilis*^{WT} group = 75.97 ± 5.05, *P. mirabilis*$^{\Delta MrpA}$ group = 83.08 ± 0.58 *P. mirabilis*$^{\Delta HpmA}$ group = 93.09 ± 2.87, *P. mirabilis*$^{\Delta UreC}$ group = 80.40 ± 2.99; F (4, 35) = 9.981, P = 0.0002, one-way ANOVA measures; P value compared to Normal group: *P. mirabilis*^{WT}, P = 0.0002, *P. mirabilis*$^{\Delta HpmA}$, P = 0.3294, Dunnett's posthoc test). We also found that the dopaminergic neuronal cells in the SNpc were degenerated by *P. mirabilis*-treated mice, excluding those treated with *P. mirabilis*$^{\Delta HpmA}$ (mean ± SEM,

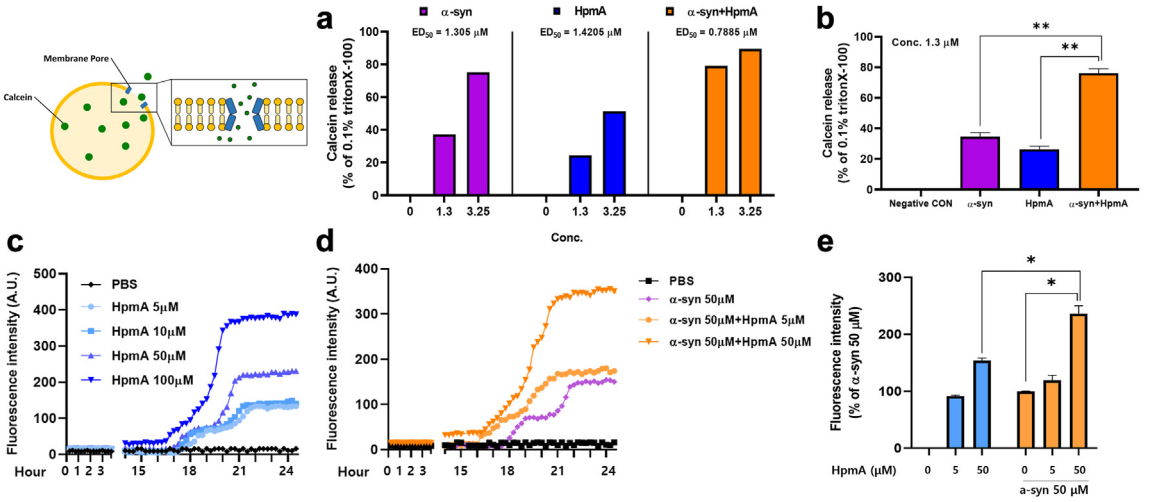

Fig. 6: **Haemolysin A oligomerises itself and induces pore formation in the plasma membrane**. (a and b) Leakage assay using α-syn, haemolysin A (HpmA), and co-incubated α-syn and HpmA. (a) 50% Efficacy dosage (ED_{50}) of each protein (N = 3 per group). (b) Comparison between single treatment and co-incubated treatment (N = 3). (c–e) Th-T assay for β-sheet aggregation using (c) HpmA, (d and e) α-syn and HpmA co-incubated every 15 min for 24 h (N = 3 per group). Data are presented as mean with error bars, SEM. Statistical analyses were performed by two-tailed t-test. Statistical significances were indicated by * P < 0.05 and ** P < 0.01. This experiment was repeated twice.

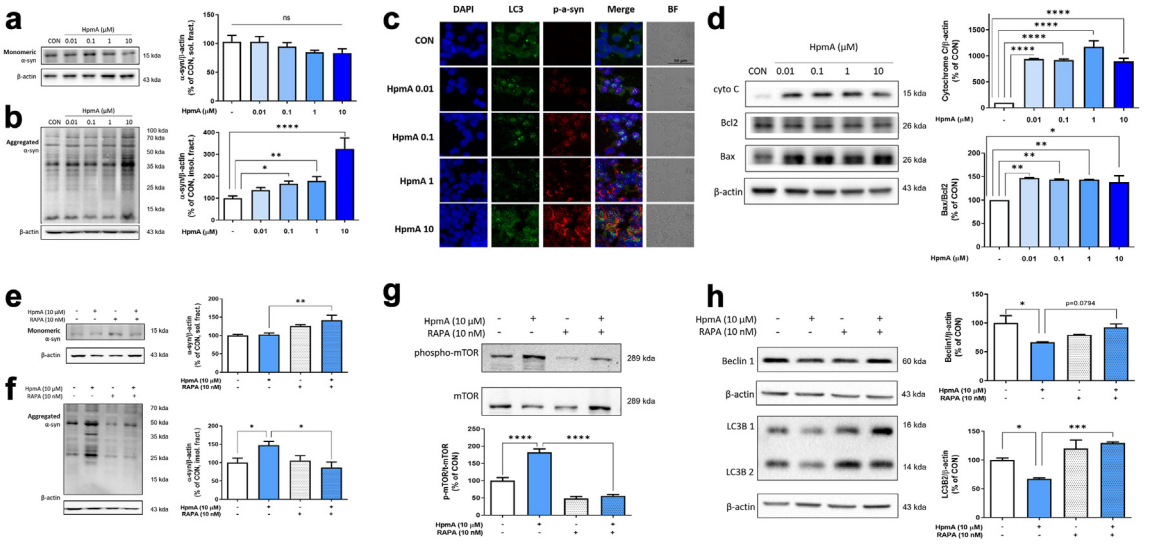

Fig. 7: **Haemolysin A exacerbates intestinal synucleinopathy by autophagic disruption**. Representative Western blot analysis for the expression of α-syn in STC-1 cells. Proteins were fractionated by 10% Triton X-100 contained PBS. The soluble fraction was used for monomeric α-syn and the insoluble fraction was used for aggregated α-syn. The ratio of each band density to that of β-actin was calculated and the relative expression levels were normalised by the normal group. (a) Expression of Triton X-100-soluble α-syn in haemolysin A (HpmA)-treated STC-1 cells (N = 4 per group). (b) Expression of Triton X-100-soluble α-syn in HpmA-treated STC-1 cells (N = 4 per group). (c) Representative analysis of immunofluorescence for the expression of LC3 (Green) and phosphorylated α-syn (Red) in HpmA-treated STC-1 cells (N = 4 × per group, 1200 × magnification, scale bar = 50 μm). (d) Analysis of bax, bcl2, and cytochrome C in HpmA-treated STC-1 cells by Western blot (N = 4 per group). (e) Expression of Triton X-100-soluble α-syn in HpmA or/and Rapamycin (RAPA)-treated STC-1 cells (N = 4 per group). (f) Expression of Triton X-100-soluble α-syn in HpmA or/and RAPA-treated STC-1 cells (N = 4 per group). (g) Analysis of phosphorylated mTOR in HpmA or/and RAPA-treated STC-1 cells by Western blot (N = 4). (h) Analysis of Beclin1, LC3B in HpmA or/and RAPA-treated STC-1 cells by Western blot (N = 4 per group). The ratio of each band density to that of β-actin was calculated and the relative expression levels were normalised by the normal group. Data are presented as mean with error bars, SEM. Statistical analyses were performed by one-way ANOVA with Dunnett's multiple comparison test. Statistical significances were indicated by * P < 0.05, ** P < 0.01, *** P < 0.001 and **** P < 0.0001. This experiment was repeated twice.

cells/mm^3; Normal group = 4735.00 ± 362.90, *P. mirabilis*^{WT} group = 2921.00 ± 72.60, *P. mirabilis*$^{\Delta MrpA}$ group = 3724.00 ± 179.90, *P. mirabilis*$^{\Delta HpmA}$ group = 4060.00 ± 276.40, *P. mirabilis*$^{\Delta UreC}$ group = 3134.00 ± 221.60; F (4, 35) = 8.599, P = 0.0001, one-way ANOVA measures; P value compared to Normal group: *P. mirabilis*^{WT}, P < 0.0001, *P. mirabilis*$^{\Delta HpmA}$, P = 0.5561, Dunnett's posthoc test). In contrast, there was no change in TH-positive signals in either the ST or SNpc of *P. mirabilis*$^{\Delta HpmA}$-treated mice compared to those of normal mice (P value compared to TH-positive signals in *P. mirabilis*$^{\Delta HpmA}$ group mouse ST: *P. mirabilis*^{WT}, P = 0.0079; *P. mirabilis*$^{\Delta MrpA}$, P = 0.1009; *P. mirabilis*$^{\Delta UreC}$, P = 0.0203, Dunnett's posthoc test. P value compared to TH-positive cells in *P. mirabilis*$^{\Delta HpmA}$ group mouse SNpc: *P. mirabilis*^{WT}, P < 0.0001; *P. mirabilis*$^{\Delta MrpA}$, P = 0.0575; *P. mirabilis*$^{\Delta UreC}$, P = 0.0012, Dunnett's posthoc test; Fig. 3d–f). Neuroinflammation is another major pathological characteristic of *P. mirabilis*. As shown in Fig. 3g and h, *P. mirabilis* increased microglial expression to 222% in the mouse SNpc compared to the normal group (mean ± SEM, cells/mm^3; Normal group = 1117.00 ± 190.10, *P. mirabilis*^{WT} group = 2481.00 ± 233.40, *P. mirabilis*$^{\Delta MrpA}$ group = 1807.00 ± 240.50, *P. mirabilis*$^{\Delta HpmA}$ group = 1157.00 ± 173.90, *P. mirabilis*$^{\Delta UreC}$ group = 2028.00 ± 134.90; F (4, 35) = 8.380, P = 0.0002, one-way ANOVA measures; P value compared to Normal group: *P. mirabilis*^{WT}, P = 0.0003, *P. mirabilis*$^{\Delta HpmA}$, P = 0.9997, Dunnett's posthoc test); otherwise, it was significantly suppressed by normal levels when treated with *P. mirabilis*$^{\Delta HpmA}$ (P value compared to *P. mirabilis*$^{\Delta HpmA}$ group: *P. mirabilis*^{WT}, P = 0.0006; *P. mirabilis*$^{\Delta MrpA}$, P = 0.0952; *P. mirabilis*$^{\Delta UreC}$, P = 0.0140, Dunnett's posthoc test). In addition, we analysed microglial morphology in the SN to confirm microglial activation. Activated microglia were observed in mice administered with other strains, except for mice administered with HpmA-mutated *P. mirabilis* (Supplementary Fig. S2).

HpmA in *P. mirabilis* induces α-syn aggregation in both the mouse brain and intestine

We examined the aggregation of α-syn in the mouse SNpc using immunofluorescence. Except for the mice administered with *P. mirabilis*$^{\Delta HpmA}$, deletion of MrpA and UreC did not inhibit *P. mirabilis*-induced α-syn aggregation. α-syn aggregation in the brain was increased by more than 300% compared to that of normal mice (mean ± SEM, cells/mm^3; Normal group = 802.10 ± 91.46, *P. mirabilis*^{WT} group = 3114.00 ± 283.80, *P. mirabilis*$^{\Delta MrpA}$ group = 2482.00 ± 277.00, *P. mirabilis*$^{\Delta HpmA}$ group = 814.90 ± 121.10, *P. mirabilis*$^{\Delta UreC}$ group = 2400.00 ± 470.40; F (4, 35) = 9.497, P = 0.0005, one-way ANOVA measures; P values compared with Normal group: *P. mirabilis*^{WT}, P = 0.0009, *P. mirabilis*$^{\Delta HpmA}$, P > 0.9999, Dunnett's posthoc test. P value compared to *P. mirabilis*$^{\Delta HpmA}$ group: *P. mirabilis*^{WT}, P = 0.0009; *P. mirabilis*$^{\Delta MrpA}$, P = 0.0069; *P. mirabilis*$^{\Delta UreC}$, P = 0.0167, Dunnett's posthoc test; Fig. 4a and b). Likewise, the expression of proteinase K-resistant α-syn in both ST and SNpc showed a tendency similar to that of immunofluorescence. In the ST, except for *P. mirabilis*$^{\Delta HpmA}$ (mean ± SEM, % of Normal group; 98.04 ± 14.37%), *P. mirabilis*^{WT}, *P. mirabilis*$^{\Delta MrpA}$ and *P. mirabilis*$^{\Delta UreC}$ increased proteinase K-resistant α-syn optical density by 172.60 ± 7.09, 182.10 ± 15.61, and 212.40 ± 6.41, respectively (F (4, 35) = 19.58, P < 0.0001, one-way ANOVA measures; P value compared to Normal group: *P. mirabilis*^{WT}, P = 0.0005, *P. mirabilis*$^{\Delta HpmA}$, P = 0.9998, Dunnett's posthoc test. P value compared to *P. mirabilis*$^{\Delta HpmA}$ group: *P. mirabilis*^{WT}, P = 0.0004; *P. mirabilis*$^{\Delta MrpA}$, P < 0.0001; *P. mirabilis*$^{\Delta UreC}$, P < 0.0001, Dunnett's posthoc test; Fig. 4a and b). In the SN, the optical density of proteinase K-resistant α-syn was upregulated by *P. mirabilis*^{WT}, *P. mirabilis*$^{\Delta MrpA}$ and *P. mirabilis*$^{\Delta UreC}$ to 122.20 ± 6.09, 117.70 ± 4.66 and 125.60 ± 3.01%, respectively, compared to the normal. (*P. mirabilis*$^{\Delta HpmA}$ group = 104.00 ± 5.26% of Normal group; F (4, 35) = 5.520, P = 0.0012, one-way ANOVA measures; P value compared to Normal group: *P. mirabilis*^{WT}, P = 0.0053, *P. mirabilis*$^{\Delta HpmA}$, P = 0.9437, Dunnett's posthoc test. P values compared to *P. mirabilis*$^{\Delta HpmA}$ group: *P. mirabilis*^{WT}, P = 0.0383; *P. mirabilis*$^{\Delta MrpA}$, P = 0.1555; *P. mirabilis*$^{\Delta UreC}$, P = 0.0165, Dunnett's posthoc test; Fig. 4c–e). To understand the effects of HpmA, additional assessments were performed using the mice that were gavaged with HpmA-expressing *E. coli* (*E. coli*$^{HpmA+/+}$; Supplementary Fig. S3a). Motor function and brain dopaminergic neurones, microglia, or α-syn inclusions were partially deteriorated by the administration of *E. coli*$^{HpmA+/+}$ (Supplementary Fig. S3b–i).

To estimate *P. mirabilis*-derived major factors that affect intestinal α-syn aggregation, we performed dot blot analyses to evaluate the expression of α-syn aggregates in the mouse colon. *P. mirabilis*-treated mice showed a significant 147% increase in colonic α-syn aggregation compared with that of normal mice (mean ± SEM, α-syn/β-actin intensity: normal = 0.6179 ± 0.0281, *P. mirabilis*^{WT} group = 0.9856 ± 0.0428; F (4, 35) = 4.603, P = 0.0080, one-way ANOVA measures). These effects were maintained in the colon of mouse that were gavaged with *P. mirabilis*$^{\Delta MrpA}$ and *P. mirabilis*$^{\Delta UreC}$ (mean ± SEM, α-syn/β-actin intensity: *P. mirabilis*$^{\Delta MrpA}$ = 0.9190 ± 0.0814, *P. mirabilis*$^{\Delta UreC}$ group = 0.8948 ± 0.1577), with the exception of *P. mirabilis*$^{\Delta HpmA}$ (α-syn intensity: 0.5620 ± 0.0961; P values compared to Normal group: *P. mirabilis*^{WT}, P = 0.0251, *P. mirabilis*$^{\Delta HpmA}$, P = 0.9761, Dunnett's posthoc test. P values compared to *P. mirabilis*$^{\Delta HpmA}$ group: *P. mirabilis*^{WT}, P = 0.0123; *P. mirabilis*$^{\Delta MrpA}$, P = 0.0381; *P. mirabilis*$^{\Delta UreC}$, P = 0.565, Dunnett's posthoc test; Fig. 5a and b). Furthermore, we confirmed these results by fractionating the solubility of

α-syn by Triton-X100. There were no significant differences of α-syn expression in triton-X100 soluble fraction between *P. mirabilis* mutant types-treated mice (F (4, 35) = 2.753, P = 0.07, one-way ANOVA measures). On the other hand, intestinal insoluble α-syn expressions were significantly increased by *P. mirabilis*^{WT}, *P. mirabilis*$^{\Delta MrpA}$, and *P. mirabilis*$^{\Delta UreC}$, but not by *P. mirabilis*$^{\Delta HpmA}$ (mean ± SEM, % of Normal group; Normal group = 100.00 ± 6.06, *P. mirabilis*^{WT} group = 137.30 ± 4.65, *P. mirabilis*$^{\Delta MrpA}$ group = 150.60 ± 4.11, *P. mirabilis*$^{\Delta HpmA}$ group = 115.10 ± 4.18, *P. mirabilis*$^{\Delta UreC}$ group = 135.60 ± 3.87% of normal group; F (4, 35) = 18.59, P < 0.0001, one-way ANOVA measures; P value compared to Normal group: *P. mirabilis*^{WT}, P = 0.0002, *P. mirabilis*$^{\Delta HpmA}$, P = 0.1092, Dunnett's posthoc test. P value compared to *P. mirabilis*$^{\Delta HpmA}$ group: *P. mirabilis*^{WT}, P = 0.0141; *P. mirabilis*$^{\Delta MrpA}$, P = 0.0003; *P. mirabilis*$^{\Delta UreC}$, P = 0.0235, Dunnett's posthoc test; Fig. 5c–e). We found that the aggregation of α-syn in enteroendocrine cells was induced by a *P. mirabilis*-sonicated supernatant solution (Supplementary Fig. S4a) as well as by mutated *P. mirabilis*, excluding HpmA, *in vitro* (Supplementary Fig. S4b), supporting the idea that the secreted virulence factor had more effects on PD pathology than those with attached bacterial walls.

HpmA oligomerises itself and induces pore formation in the plasma membrane and aggregation of α-syn

Oligomerisation of α-syn with a ring-like appearance is known to be toxic. Proteins contained in the haemolysin class (e.g. α-haemolysin from *S. aureus*) are known as bacterial virulence factors that can arrange into a lipid-soluble toxin with a transmembrane barrel; however, the molecular mechanisms of HpmA derived from *P. mirabilis* have not been elucidated. Before deducing the possible mechanisms underlying the effects of HpmA on PD pathology, we performed a leakage assay to evaluate whether HpmA could insert pores into the plasma membrane. As shown in Fig. 6a, HpmA significantly increased membrane permeability in a dose-dependent manner (ED_{50} = 1.4205 μM). Moreover, A11 immunoreactivity was observed to determine whether HpmA oligomerized, resulting in pore formation. After incubation with HpmA for aggregation, the A11 antibody recognised HpmA pores in a dose-dependent manner (Supplementary Fig.S5a). Moreover, to examine the amyloidogenic nature of HpmA aggregation, we measured time-dependent changes to the extent of β-sheet aggregation using the Th-T fluorescence assay. The fluorescence intensity increased with HpmA during incubation (Fig. 6c).

Our next step was to determine if the oligomerisation of HpmA could induce the aggregation of α-syn. Pore formation significantly increased in the plasma membrane when HpmA co-incubated with α-syn by more than 2-fold compared to each single treatment (Calcein release: α-syn = 34.46 ± 1.52, HpmA = 26.42 ± 1.14, α-syn + HpmA = 79.05 ± 3.67% of 0.1% tritonX-100; P value compared to α-syn + HpmA group: α-syn, P = 0.0026; HpmA, P = 0.0016; two-tailed unpaired t-test; Fig. 6a and b, Supplementary Fig.S6). Western blotting showed that, HpmA and α-syn monomer did not react with each other's antibodies. Surprisingly, immunoreactivity with the anti-A11 antibody increased in the co-incubated condition compared to that in the monomeric condition (Supplementary Fig. S5b). Th-T fluorescent signals significantly increased with co-incubation with each other rather than the single condition (mean ± SEM, % of α-syn 50 μM fluorescence intensity: HpmA 5 μM = 91.75 ± 1.32, HpmA 50 μM = 153.80 ± 4.62, α-syn 50 μM = 100.00 ± 0.33, α-syn 50 μM + HpmA 5 μM = 119.50 ± 8.58, α-syn 50 μM + HpmA 5 μM = 119.50 ± 8.58; P value compared to α-syn 50 μM + HpmA 5 μM group: HpmA 50 μM, P = 0.0300; α-syn 50 μM, P = 0.0102; two-tailed unpaired t-test; Fig. 6d and e). These results indicated the possible effects of HpmA on aggregation during oligomerisation.

HpmA exacerbates intestinal synucleinopathy by autophagic disruption

Membrane pore formation induces an increase in intracellular calcium influx, resulting in oligomerisation and neuronal cell death. To estimate the biological changes induced by HpmA, especially in enteric neurones, STC-1, an enteric neurone-like cell line, was used in subsequent studies.[24] When HpmA was treated in intestinal cells, α-syn was significantly aggregated into oligomers and a soluble-phosphorylated form in a dose-dependent manner and expressions were increased up to 324% compared to those of the normal (Monomeric α-syn: F (4, 15) = 1.261, P = 0.3284, one-way ANOVA measures. Aggregated α-syn (mean ± SEM, % of Control group): Control = 100.00 ± 10.66, HpmA 0.01 μM = 136.50 ± 11.20, HpmA 0.1 μM = 165.00 ± 12.79, HpmA 1 μM = 178.10 ± 19.98, HpmA 10 μM = 324.90 ± 49.43, F (4, 15) = 11.370, P = 0.0002, one-way ANOVA measures; P value compared to the control group: HpmA 0.01 μM, P = 0.2131; HpmA 0.1 μM, P = 0.0182; HpmA 1 μM, P = 0.0056; HpmA 10 μM, P < 0.0001; Dunnett's post-hoc test; Fig. 7a–c). We found that phosphor-α-syn increased by HpmA with the increase of nucleus LC3B (Fig. 7c). The accumulation of α-syn results in cell disruption, such as mitochondrial dysfunction. When treated with HpmA in the enteroendocrine cells, the ratio of Bax to Bcl 2 and the protein expression of cytochrome C significantly increased up to 1.47-fold and 11.72-fold compared to the control (Ratio of Bax to Bcl2 (mean ± SEM, % of Control group): HpmA 0.01 μM = 147.10 ± 0.59, HpmA 0.1 μM = 143.40 ± 1.45, HpmA 1 μM = 143.50 ± 0.18, HpmA

10 μM = 138.40 ± 13.30; Cytochrome C (mean ± SEM, % of Control group): HpmA 0.01 μM = 942.00 ± 5.83, HpmA 0.1 μM = 918.40 ± 20.16, HpmA 1 μM = 1172.00 ± 118.20, HpmA 10 μM = 894.90 ± 57.96; Ratio of Bax to Bcl2 (mean ± SEM, % of Control group): F (4, 15) = 5.224, P = 0.0099, one-way ANOVA measures; P value compared to the control group: HpmA 0.01 μM, P = 0.0030; HpmA 0.1 μM, P = 0.0056; HpmA 1 μM, P = 0.0055; HpmA 10 μM, P = 0.0127; Cytochrome C: F (4, 15) = 24.11, P < 0.0001, one-way ANOVA measures; P value compared to the control group: HpmA 0.01 μM, P < 0.0001; HpmA 0.1 μM, P < 0.0001; HpmA 1 μM, P < 0.0001; HpmA 10 μM, P < 0.0001; Dunnett's posthoc test); however, a dose-dependent increase was not been observed (Fig. 7d).

It was inferred that HpmA treatment induced α-syn aggregation by LC3B and mitochondrial dysfunction. To investigate this specific mechanism, we attempted to confirm changes in the expression of autophagy-related factors at the RNA level in HpmA-treated STC-1 cells. As a result, it was confirmed that the expression level of Atg proteins involved in mTOR-mediated signalling was significantly decreased (Supplementary Fig. S7). Based on this, we expected that HpmA would stimulate mTOR-mediated signalling in biological intestinal samples. The results showed that phosphorylation of mTOR was significantly increased by HpmA at a concentration of 10 μM (mean ± SEM, % of Control group; 182.10 ± 10.05%; F (4, 15) = 58.99, P < 0.0001; one-way ANOVA measures; P value compared to the control group, P < 0.0001; Dunnett's posthoc test; Fig. 7g). At the same time, the expression levels of Beclin1 and LC3B2 were also significantly decreased by HpmA treatment (Beclin1 (mean ± SEM, % of Control group): 66.48 ± 0.82; F (4, 15) = 4.386, P = 0.0292; one-way ANOVA measures; P value compared to the control group, P = 0.0155; Dunnett's posthoc test; LC3B2 (mean ± SEM, % of Control group): 67.43 ± 1.57; F (4, 15) = 10.80, P = 0.0013; one-way ANOVA measures; P value compared to the control group, P = 0.0391; Dunnett's posthoc test; Fig. 7h). Furthermore, we used the rapamycin (RAPA), an mTOR inhibitor, to investigate whether the mechanism of action of HpmA was related to mTOR signallings. We found that alterations induced by HpmA could be significantly recovered by RAPA to the normal levels (phosphor-mTOR (mean ± SEM, % of Control group): RAPA = 48.21 ± 5.78, RAPA + HpmA = 55.77 ± 3.85; P value compared to the HpmA group: RAPA + HpmA, P < 0.0001; Dunnett's posthoc test; Beclin1 (mean ± SEM, % of Control group): RAPA = 79.41 ± 0.66, RAPA + HpmA = 92.60 ± 5.80; P value compared to the HpmA group: RAPA + HpmA, P = 0.0794; Dunnett's posthoc test; LC3B2 (mean ± SEM, % of Control group): RAPA = 120.00 ± 14.78, RAPA + HpmA = 129.5 ± 2.03; P value compared to the HpmA group: RAPA + HpmA, P = 0.0010; Dunnett's posthoc test; Fig. 7g and h). These alterations resulted in the inhibition of α-syn aggregation in HpmA-treated STC-1 cells (Aggregated α-syn (mean ± SEM, % of Control group): HpmA = 147.60 ± 10.42, RAPA = 105.70 ± 13.49, RAPA + HpmA = 87.27 ± 14.51; F (4, 15) = 4.219, P = 0.0168; one-way ANOVA measures; P value compared to the control group: HpmA, P = 0.0307; Dunnett's posthoc test; P value compared to the HpmA group: RAPA + HpmA, P = 0.0116; Dunnett's posthoc test; Fig. 7f). Overall, these data suggest that HpmA induced enteric neuronal degeneration with the induction of α-syn aggregation, activation of mTOR-mediated signalling, and mitochondrial dysfunction.

Discussion

Recent studies have reported that intestinal α-syn pathology could be the part of the pathogenesis of the brain degeneration, especially for PD. Accordingly, we hypothesised that virulence factors derived from *P. mirabilis* trigger intestinal α-syn aggregation, leading to the propagation of α-syn and neurodegeneration in PD. Here, we confirmed the pathogenic effects of *P. mirabilis* and identified the specific *P. mirabilis*-derived virulence factor, HpmA, as the pathogen responsible for PD, which induces intestinal α-syn aggregation.

While previous studies have reported that pathological changes in the intestine and brain are related to the induction of neurodegeneration in *P. mirabilis*, this study aimed to verify whether *P. mirabilis*-induced neurodegeneration is caused by alterations in the intestine. We used vagotomised mice to prove that the signal transmissions of changes in the intestine occur through the vagus nerve. The results of this study indicate that the vagus nerve is involved in *P. mirabilis*-induced brain pathological alterations. However, additional investigation of other pathways is needed. In particular, the blood-circulating system, including LPS previously reported by our research team,[15,17] various immune mediators, pathological factors such as α-syn, and microbiome-derived metabolites are involved in the pathological mechanisms of brain degenerative diseases including Parkinson's disease and autism.[13,14] In particular, considering the symptoms that are seen in patients with PD, such as the leaky gut phenomenon, *P. mirabilis*-induced intestinal inflammation is expected to play a major role in neurological pathology.[23,25] These results confirmed the tendency for brain degeneration in the *E. coli* wild type (Supplementary Fig. S2). However, this was shown as an indirect result to act on motor impairment and dopaminergic neuronal death, and recently, it has been reported that α-syn pathology through the vagus nerve is closely related to the expression of PD-like phenotypes based on the gut-brain axis. Additional pathological factors were also expected to be present. In this study, we identified HpmA as a factor that can affect neurodegeneration, in addition to

LPS. When comparing the expression of factors related to LPS biosynthesis in the mutated *P. mirabilis* that was used in this study, it was confirmed that there was no difference in expression between mutated *P. mirabilis* (Supplementary Fig. S8). This suggests that other factors, such as HpmA, may play a role in the action of LPS, as seen in previous studies.

Antibiotic treatment ameliorated brain neurodegeneration that was induced by *P. mirabilis*. This suggests that *P. mirabilis*-induced neurodegeneration is achieved by the inoculation of *P. mirabilis* into the intestine. Since the antibiotics used in this study targeted gram-negative bacteria and did not eliminate only *P. mirabilis*, the possibility that they acted against strains altered by *P. mirabilis* cannot be ruled out. We measured the abundance of *P. mirabilis* according to antibiotic treatment and confirmed that antibiotics significantly decreased the abundance of *P. mirabilis* in mouse faeces (Supplementary Fig. S9). Based on this study, future research should be conducted with additional consideration of changes in the strain population in the mouse intestine and the relationship between the altered strain and neurodegeneration. However, considering that antibiotic did not induce behavioural and histological changes in normal mice,[26] it can be inferred that they appeared through the effect on strains in the intestine, not the direct effect of antibiotic drugs on the brain.

Haemolysins lyse of red blood cells by disrupting the cell membranes. Most haemolysins are pore-forming toxins that induce blood cell lysis by producing pores in the cytoplasmic membrane. They are secreted by several bacteria including, such as *Staphylococcus aureus*, *Escherichia coli*, *Vibrio parahemolyticus*, and *Proteus* spp.[27,28] HpmA, a haemolysin A, forms pores with a right-handed parallel helix with three adjoining segments of anti-parallel sheet by cooperative, β-strand interactions between HpmA265 (truncated form of HpmA) and full-length HpmA.[29] Unlike other haemolytic proteins, HpmA is secreted via a two-partner secretion pathway consisting of a passenger protein and its cognate transporter. In the case of HpmA, HpmB, the transporter of HpmA, is an essential component of its secretion, as verified with other types of haemolysins.[30,31] Althogh most strains of *P. mirabilis* secrete HpmA, there are few bacteria which secrete HpmA, such as part of *E.coli* or *Proteus* species.[32] In this case, we compared the effects of microbiota from the genus *Proteus* (Supplementary Table S2) which secretes HpmA, on the phenotypes of PD. As shown in Supplementary Fig. S1, we found that only *P. mirabilis*, secreting HpmA, induced dopaminergic neurodegeneration, α-syn aggregation, neuroinflammation, and motor impairment, though we only compared part of the *Proteus* genus. To establish such an indication, additional grounds for the secretion of HpmA by the evaluated *Proteus* strains must be presented, and additional related studies are needed.

We investigated the pathological mechanisms of HpmA on PD. Based on the concept of α-syn propagation from the gut to the brain, we focused on the interactions between HpmA and α-syn in the intestine. Recently, it was revealed that the structure of the pores of α-haemolysin works with a mechanism similar to that of amyloid proteins in membrane permeabilisation, as the hairpins in the barrel interact with the cytoplasmic membranes in a similar manner, owing to their structural and stoichiometric heterogeneity.[33,34] In this study, we demonstrated the interaction of HpmA with α-syn in lipid membranes and their oligomerization, which displayed strong reactivity to the oligomer-specific antibody A11 when both were incubated. Furthermore, it is an important result that HpmA can react with α-syn as oligomerisation and increase pore formation in cytoplasmic membrane, since the main pathological mechanism of oligomeric α-syn has been known as an interaction with the membrane to form pores, leading to cellular calcium dysregulation by an increase in intracellular calcium levels, and in turn, the accumulation of misfolded α-syn and cell death.[35,36]

This progression usually occurs in neuronal cells with the disruption of autophagosomes by the activation of mTOR-mediated signalling. Autophagosomes are essential for protein clearance. Various factors are involved in its production, and autophagy proceeds through the release of Beclin1 induced by Bcl2, including Atg proteins and the ULK complex.[37] This induces the release of LC3 into the cytosol, which is involved in protein degeneration. The mTOR is a representative regulator of autophagy. In particular, when mTOR phosphorylation is induced, factors that form the autophagosome are suppressed, and protein accumulation is promoted.[38] In addition, it is known that autophagy is inhibited through mTOR phosphorylation by the activation of TLR2 receptors, which are microbial virulence factor receptors, including α-syn.[39] These results provide evidence to support the induction of α-syn aggregation through the activation of mTOR-mediated signals of *P. mirabilis*-derived HpmA identified in this study. mTOR activated by HpmA was effectively inhibited by rapamycin, and finally, it was confirmed that α-syn aggregation was diminished. Thus, it was deduced that HpmA-induced pathological phenomena are caused by mTOR-mediated signals and various mechanisms of action, such that calcium influx and TLR2 receptor activation are expected to be possible. However, additional studies should be conducted to clearly identify these mechanisms. This study revealed that α-syn interacts with membranes to affect calcium signalling in a structure-specific manner and that oligomeric sheet-rich α-syn species ultimately lead to ENS degeneration by inhibiting autophagy. Thus, we demonstrated that the induction of pore formation in the plasma membrane accelerates intestinal α-syn aggregation by the function of HpmA in ENS-like

intestinal cells, leading to the deterioration of neurodegenerative diseases. Although part of the mechanism of action of HpmA in the intestine was identified in this study, to confirm whether the actual induction of α-syn aggregation in the intestinal cells was due to an increase in α-syn expression levels or an increase in aggregation itself, it should be verified using a SNCA-KO mouse. In addition, this study was based on the premise that HpmA promotes the aggregation of α-syn in the enteric nerve and interacts with it. Although there are neuropod cells that are known to be actually connected to the vagus nerve,[40] direct evidence on how HpmA communicates with and affects the vagus nerve must be identified through future research.

The *P. mirabilis*-induced mouse model that was used in this study is an animal model of strain-induced brain disease that is effective for explaining the gut-brain axis. The model reflects the gut-brain pathological changes that are observed in patients with degenerative brain diseases caused by intervening strains. However, some limitations need to be addressed. First, it is necessary to clarify whether the pathological changes caused by *P. mirabilis* are actually caused by *P. mirabilis* or by a chain reaction. In this study, we confirmed the mechanism of neurodegeneration by HpmA; however, HpmA is a factor included in strains other than *P. mirabilis*, and based on previous studies, LPS may also be a factor. Given that these factors are not specific to *P. mirabilis*, the possibility of changes in the colonisation of the entire strain owing to the intervention of *P. mirabilis* cannot be ruled out. Previous studies have confirmed that degeneration in the nigrostriatal dopaminergic neuronal pathway was prominent in brain neurodegeneration when *P. mirabilis* was administered. Although this is similar to the characteristics of PD, it is necessary to confirm whether it is related to the actual characteristics of PD such as non-motor symptoms and responsiveness to levodopa. In particular, additional research will be needed, showing a-syn propagation from the intestine to the brain in PD in this model by stage. Brain diseases show complex pathological phenomena that can occur according to genetic factors and the accumulation of toxic substances, and a model for this has also been established. Therefore, to study the pathology of degenerative brain diseases, including PD, various factors, including microbiota colonisation should be considered.

The results in this study suggests the possibility of a *P. mirabilis* strain that induces brain neurodegeneration but has recently been reported as involved in conditions such as Crohn's disease as well as irritable and inflammatory bowel syndrome.[41] In particular, since a correlation between intestinal inflammation and brain neuroinflammation has been reported,[42] these results can be used as basic data for research on the pathological correlation between intestinal and brain diseases. Moreover, as there have been no comparative studies on the distribution of *P. mirabilis* and the pathological progression of *P. mirabilis* according to sex, additional studies are required.

In summary, the proof-of-concept of this study supports the notion that microbiota and specific virulence factors are closely involved in α-syn pathology and neurodegeneration and that HpmA derived from *P. mirabilis* mediates this interaction, at least in part. Although further studies are required to confirm and validate these findings, our study suggests that HpmA from *P. mirabilis* is a possible pathogenic factor in neurodegenerative diseases and provides scientific evidence for the role of the gut-brain axis in brain neurodegeneration. These findings will serve as a basis for studies investigating the pathological interactions between the gut microbiota, including *P. mirabilis*, and the host.

Contributors

EH and JGC designed this study, performed the experimental work, acquired and analysed the data, and prepared and wrote the manuscript. YC, IGJ, BK, Y-JS and JMA performed the experiments and contributed to data acquisition and analyses. EH, JGC, MSO verified the underlying data. MGP, DK, SVY, SJC and DHK supervised the experiments and critically revised the manuscript. S-US and CHK provided the gene-mutated *P. mirabilis* and critically revised the manuscript. MSO designed, performed, analysed, and supervised the experiments, and wrote and revised the manuscript. MSO acted as the guarantor for the present study. All authors reviewed and approved the final version of the manuscript.

Data sharing statement

The data generated in this study are available upon request from the corresponding author.

Declaration of interests

EH, JGC, DHK and MSO are inventors with a provisional patent, "Method for diagnosing neurodegenerative disease using HpmA" that is licensed to MetaCen Therapeutics. MGP is a co-founder of MetaCen Therapeutics.

Appendix A. Supplementary data

Supplementary data related to this article can be found at https://doi.org/10.1016/j.ebiom.2023.104887.

References

1 Alexander GE. Biology of Parkinson's disease: pathogenesis and pathophysiology of a multisystem neurodegenerative disorder. *Dialogues Clin Neurosci*. 2004;6(3):259–280.

2 Noyce AJ, Lees AJ, Schrag AE. The prediagnostic phase of Parkinson's disease. *J Neurol Neurosurg Psychiatry*. 2016;87(8):871–878. https://doi.org/10.1136/jnnp-2015-311890.

3 Braak H, Rub U, Gai WP, Del Tredici K. Idiopathic Parkinson's disease: possible routes by which vulnerable neuronal types may be subject to neuroinvasion by an unknown pathogen. *J Neural Transm*. 2003;110(5):517–536. https://doi.org/10.1007/s00702-002-0808-2.

4 Braak H, Del Tredici K, Rub U, de Vos RA, Jansen Steur EN, Braak E. Staging of brain pathology related to sporadic Parkinson's disease. *Neurobiol Aging*. 2003;24(2):197–211. https://doi.org/10.1016/s0197-4580(02)00065-9.

5 Liu B, Fang F, Pedersen NL, et al. Vagotomy and Parkinson disease: a Swedish register-based matched-cohort study. *Neurology*. 2017;88(21):1996–2002. https://doi.org/10.1212/WNL.0000000000003961.

6 Svensson E, Horvath-Puho E, Thomsen RW, et al. Vagotomy and subsequent risk of Parkinson's disease. *Ann Neurol*. 2015;78(4):522–529. https://doi.org/10.1002/ana.24448.

7 Ulusoy A, Rusconi R, Perez-Revuelta BI, et al. Caudo-rostral brain spreading of alpha-synuclein through vagal connections. *EMBO Mol Med*. 2013;5(7):1119–1127. https://doi.org/10.1002/emmm.201302475.
8 Visanji NP, Brooks PL, Hazrati LN, Lang AE. The prion hypothesis in Parkinson's disease: braak to the future. *Acta Neuropathol Commun*. 2013;1:2. https://doi.org/10.1186/2051-5960-1-2.
9 Holmqvist S, Chutna O, Bousset L, et al. Direct evidence of Parkinson pathology spread from the gastrointestinal tract to the brain in rats. *Acta Neuropathol*. 2014;128(6):805–820. https://doi.org/10.1007/s00401-014-1343-6.
10 Kim S, Kwon SH, Kam TI, et al. Transneuronal propagation of pathologic alpha-synuclein from the gut to the brain models Parkinson's disease. *Neuron*. 2019;103(4):627–641.e7. https://doi.org/10.1016/j.neuron.2019.05.035.
11 Borghammer P, Van Den Berge N. Brain-first versus gut-first Parkinson's disease: a hypothesis. *J Parkinsons Dis*. 2019;9(s2):S281–S295. https://doi.org/10.3233/JPD-191721.
12 Horsager J, Andersen KB, Knudsen K, et al. Brain-first versus body-first Parkinson's disease: a multimodal imaging case-control study. *Brain*. 2020;143(10):3077–3088. https://doi.org/10.1093/brain/awaa238.
13 Needham BD, Kaddurah-Daouk R, Mazmanian SK. Gut microbial molecules in behavioural and neurodegenerative conditions. *Nat Rev Neurosci*. 2020;21(12):717–731. https://doi.org/10.1038/s41583-020-00381-0.
14 Morais LH, Schreiber HL, Mazmanian SK. The gut microbiota-brain axis in behaviour and brain disorders. *Nat Rev Microbiol*. 2021;19(4):241–255. https://doi.org/10.1038/s41579-020-00460-0.
15 Gorecki AM, Preskey L, Bakeberg MC, et al. Altered gut microbiome in Parkinson's disease and the influence of Lipopolysaccharide in a human alpha-synuclein over-expressing mouse model. *Front Neurosci*. 2019;13:839. https://doi.org/10.3389/fnins.2019.00839.
16 Sampson TR, Challis C, Jain N, et al. A gut bacterial amyloid promotes alpha-synuclein aggregation and motor impairment in mice. *Elife*. 2020;9. https://doi.org/10.7554/eLife.53111.
17 Choi JG, Kim N, Ju IG, et al. Oral administration of proteus mirabilis damages dopaminergic neurons and motor functions in mice. *Sci Rep*. 2018;8(1):1275. https://doi.org/10.1038/s41598-018-19646-x.
18 Seo SU, Kamada N, Munoz-Planillo R, et al. Distinct commensals induce interleukin-1 beta via NLRP3 inflammasome in inflammatory monocytes to promote intestinal inflammation in response to injury. *Immunity*. 2015;42(4):744–755. https://doi.org/10.1016/j.immuni.2015.03.004.
19 Gisby J, Wightman BJ, Beale AS. Comparative efficacies of ciprofloxacin, amoxicillin, amoxicillin-clavulanic acid, and cefaclor against experimental Streptococcus pneumoniae respiratory infections in mice. *Antimicrob Agents Chemother*. 1991;35(5):831–836. https://doi.org/10.1128/AAC.35.5.831.
20 Bakker-Woudenberg IA, ten Kate MT, Guo L, Working P, Mouton JW. Improved efficacy of ciprofloxacin administered in polyethylene glycol-coated liposomes for treatment of Klebsiella pneumoniae pneumonia in rats. *Antimicrob Agents Chemother*. 2001;45(5):1487–1492. https://doi.org/10.1128/AAC.45.5.1487-1492.2001.
21 Tatulian SA, Kandel N. Membrane pore formation by peptides studied by fluorescence techniques. *Methods Mol Biol*. 2019;2003:449–464. https://doi.org/10.1007/978-1-4939-9512-7_19.
22 Bate ST, Clark RA, Stanford SC. Using InVivoStat to perform the statistical analysis of experiments. *J Psychopharmacol*. 2017;31(6):644–652. https://doi.org/10.1177/0269881116682213.
23 Zhang J, Hoedt EC, Liu Q, et al. Elucidation of proteus mirabilis as a key bacterium in crohn's disease inflammation. *Gastroenterology*. 2021;160(1):317–330.e11. https://doi.org/10.1053/j.gastro.2020.09.036.
24 Chandra R, Hiniker A, Kuo YM, Nussbaum RL, Liddle RA. alpha-Synuclein in gut endocrine cells and its implications for Parkinson's disease. *JCI Insight*. 2017;2(12). https://doi.org/10.1172/jci.insight.92295.
25 Zhu M, Liu X, Ye Y, et al. Gut microbiota: a novel therapeutic target for Parkinson's disease. *Front Immunol*. 2022;13:937555. https://doi.org/10.3389/fimmu.2022.937555.
26 Sampson TR, Debelius JW, Thron T, et al. Gut microbiota regulate motor deficits and neuroinflammation in a model of Parkinson's disease. *Cell*. 2016;167(6):1469–1480.e12. https://doi.org/10.1016/j.cell.2016.11.018.
27 Dal Peraro M, van der Goot FG. Pore-forming toxins: ancient, but never really out of fashion. *Nat Rev Microbiol*. 2016;14(2):77–92. https://doi.org/10.1038/nrmicro.2015.3.
28 Yamashita D, Sugawara T, Takeshita M, et al. Molecular basis of transmembrane beta-barrel formation of staphylococcal pore-forming toxins. *Nat Commun*. 2014;5:4897. https://doi.org/10.1038/ncomms5897.
29 Weaver TM, Hocking JM, Bailey LJ, et al. Structural and functional studies of truncated hemolysin A from proteus mirabilis. *J Biol Chem*. 2009;284(33):22297–22309. https://doi.org/10.1074/jbc.M109.014431.
30 Guerin J, Bigot S, Schneider R, Buchanan SK, Jacob-Dubuisson F. Two-partner secretion: combining efficiency and simplicity in the secretion of large proteins for bacteria-host and bacteria-bacteria interactions. *Front Cell Infect Microbiol*. 2017;7:148. https://doi.org/10.3389/fcimb.2017.00148.
31 Holland IB, Schmitt L, Young J. Type 1 protein secretion in bacteria, the ABC-transporter dependent pathway (review). *Mol Membr Biol*. 2005;22(1-2):29–39. https://doi.org/10.1080/09687860500042013.
32 Cestari SE, Ludovico MS, Martins FH, da Rocha SP, Elias WP, Pelayo JS. Molecular detection of HpmA and HlyA hemolysin of uropathogenic Proteus mirabilis. *Curr Microbiol*. 2013;67(6):703–707. https://doi.org/10.1007/s00284-013-0423-5.
33 Wu J, Blum TB, Farrell DP, DiMaio F, Abrahams JP, Luo J. Cryo-electron microscopy imaging of alzheimer's amyloid-beta 42 oligomer displayed on a functionally and structurally relevant scaffold. *Angew Chem Int Ed Engl*. 2021;60(34):18680–18687. https://doi.org/10.1002/anie.202104497.
34 Yoshiike Y, Kayed R, Milton SC, Takashima A, Glabe CG. Pore-forming proteins share structural and functional homology with amyloid oligomers. *NeuroMolecular Med*. 2007;9(3):270–275. https://doi.org/10.1007/s12017-007-0003-6.
35 Kim HY, Cho MK, Kumar A, et al. Structural properties of pore-forming oligomers of alpha-synuclein. *J Am Chem Soc*. 2009;131(47):17482–17489. https://doi.org/10.1021/ja9077599.
36 Tsigelny IF, Sharikov Y, Wrasidlo W, et al. Role of alpha-synuclein penetration into the membrane in the mechanisms of oligomer pore formation. *FEBS J*. 2012;279(6):1000–1013. https://doi.org/10.1111/j.1742-4658.2012.08489.x.
37 Maier HJ, Britton P. Involvement of autophagy in coronavirus replication. *Viruses*. 2012;4(12):3440–3451. https://doi.org/10.3390/v4123440.
38 Tsai SC, Yang JS, Peng SF, et al. Bufalin increases sensitivity to AKT/mTOR-induced autophagic cell death in SK-HEP-1 human hepatocellular carcinoma cells. *Int J Oncol*. 2012;41(4):1431–1442. https://doi.org/10.3892/ijo.2012.1579.
39 Kim C, Rockenstein E, Spencer B, et al. Antagonizing neuronal toll-like receptor 2 prevents synucleinopathy by activating autophagy. *Cell Rep*. 2015;13(4):771–782. https://doi.org/10.1016/j.celrep.2015.09.044.
40 Kaelberer MM, Buchanan KL, Klein ME, et al. A gut-brain neural circuit for nutrient sensory transduction. *Science*. 2018;361(6408). https://doi.org/10.1126/science.aat5236.
41 Abdukhakimova D, Dossybayeva K, Poddighe D. Fecal and duodenal microbiota in pediatric celiac disease. *Front Pediatr*. 2021;9:652208. https://doi.org/10.3389/fped.2021.652208.
42 Giuffre M, Gazzin S, Zoratti C, et al. Celiac disease and neurological manifestations: from gluten to neuroinflammation. *Int J Mol Sci*. 2022;23(24). https://doi.org/10.3390/ijms232415564.